Citation: Cell Death and Disease (2012) 3, e404; doi:10.1038/cddis.2012.130

www.nature.com/cddis

Bcl-2 family member Bcl-G is not a proapoptotic protein

M Giam[1,2], T Okamoto[1,2,3], JD Mintern[1,2,4], A Strasser[1,2] and P Bouillet[1,2]

The three major subgroups of the Bcl-2 family, including the prosurvival Bcl-2-like proteins, the proapoptotic Bcl-2 homology (BH)3-only proteins and Bax/Bak proteins, regulate the mitochondrial apoptotic pathway. In addition, some outliers within the Bcl-2 family do not fit into these subgroups. One of them, Bcl-G, has a BH2 and a BH3 region, and was proposed to trigger apoptosis. To investigate the physiological role of Bcl-G, we have inactivated the gene in the mouse and generated monoclonal antibodies to determine its expression. Although two isoforms of Bcl-G exist in human, only one is found in mice. mBcl-G is expressed in a range of epithelial as well as in dendritic cells. Loss of Bcl-G did not appear to affect any of these cell types. mBcl-G only binds weakly to prosurvival members of the Bcl-2 family, and in a manner that is independent of its BH3 domain. To understand what the physiological role of Bcl-G might be, we searched for Bcl-G-binding partners through immunoprecipitation/mass spectroscopy and yeast-two-hybrid screening. Although we did not uncover any Bcl-2 family member in these screens, we found that Bcl-G interacts specifically with proteins of the transport particle protein complex. We conclude that Bcl-G most probably does not function in the classical stress-induced apoptosis pathway, but rather has a role in protein trafficking inside the cell.

Cell Death and Disease (2012) **3**, e404; doi:10.1038/cddis.2012.130; published online 11 October 2012
Subject Category: Cancer

Proteins of the Bcl-2 family are divided into three subgroups according to their function and the presence of characteristic Bcl-2 homology (BH) domains. The prosurvival members (Bcl-2, Bcl-x_L, Bcl-w, Mcl-1 and A1/Bfl-1) contain four BH domains and are critical for cell survival. The proapoptotic proteins Bax and Bak, which also contain all four BH domains and are structurally similar to their prosurvival relatives, are essential for mitochondrial outer membrane permeabilisation. The BH3-only proteins (Bim, Bid, Puma, Bmf, Bik, Bad, Noxa and Hrk) are essential initiators of apoptosis that cause activation of Bax and Bak, either directly or indirectly by binding to and blocking the prosurvival Bcl-2 family members.[1] The presence of the BH1, BH2 and BH3 domains in the multi-domain proteins determines their three-dimensional structure, in particular the existence on their surface of a groove that functions as a receptor for the BH3 domain of BH3-only or the Bax/Bak proteins. Mutations in the conserved residues of the BH3 domain of proapoptotic proteins almost invariably modify or abrogate their interaction with the groove of the prosurvival Bcl-2-like proteins.[2]

A number of other proteins harbouring a BH3-like domain (and sometimes another BH domain) have been described.[3] Although many of these proteins have been included in the Bcl-2 family, their role in stress-induced apoptosis is often controversial, and some of these proteins have even been implicated in diverse non-apoptotic cellular functions, such as cell cycle regulation, DNA repair, ubiquitination, metabolism or autophagy.[3]

BCL-G, also known as BCL2L14, was first described as a novel proapoptotic member of the Bcl-2 family.[4] The human *BCL-G* gene encodes two major isoforms, BCL-G_L and BCL-G_S. BCL-G_L contains both BH3 and BH2 domains, whereas BCL-G_S contains only the BH3 domain. BCL-G_S was reported to kill cells by binding and neutralisation of prosurvival BCL-X_L. In contrast, BCL-G_L did not bind BCL-X_L and showed only poor killing activity.[4] Mouse Bcl-G is 68% identical and 78% similar to human BCL-G_L.[5] Functional characterisation of mBcl-G has been limited, and most studies have considered its proapoptotic nature as a fait accompli.

To characterise this unusual member of the Bcl-2 family, we have generated highly specific monoclonal antibodies (mAb) and Bcl-G-deficient mice. Our results highlight differences between the mouse and human *Bcl-G* genes and suggest that Bcl-G may not function as a classical BH3-only protein.

[1]The Walter and Eliza Hall Institute of Medical Research, Melbourne, VIC, Australia and [2]Department of Medical Biology, University of Melbourne, Melbourne, VIC, Australia
*Corresponding author: P Bouillet, The Walter and Eliza Hall Institute of Medical Research, Molecular Genetics of Cancer Division, 1G Royal Parade, Parkville, VIC 3052, Australia. Tel: +61 3 9345 2334; Fax: +61 3 9347 0852; E-mail: bouillet@wehi.edu.au
[3]Current address: Department of Molecular Virology, Research Institute for Microbial Diseases, Osaka University, Osaka, Japan.
[4]Current address: Department of Biochemistry and Molecular Biology, University of Melbourne, Melbourne, VIC, Australia.
Keywords: apoptosis; Bcl-G; Bcl-2 family
Abbreviations: BH, Bcl-2 homology domain; cDC, conventional dendritic cell; pDC, plasmacytoid dendritic cell; HA, haemagglutinin; mAb, monoclonal antibody; DMEM, Dulbecco's modified Eagle's medium; Y2H, yeast two-hybrid; TRAPP, transport particle protein
Received 25.7.12; accepted 25.7.12; Edited by G Melino

Results

Generation of Bcl-G-deficient mice. Targeting of the mouse *Bcl-G* gene in embryonic stem (ES) cells was achieved by introducing loxP sites flanking the ATG-containing exon 3 (Figure 1a). Hygromycin-resistant Bruce 4 clones were isolated and their genomic DNA analysed by Southern blotting (Figure 1b). *Bcl-G* gene-targeted mice were established and maintained on an inbred C57BL/6 genetic background, and were genotyped by PCR (Figure 1c). *Bcl-G*$^{-/-}$ mice were born at the expected Mendelian frequency from intercross matings of *Bcl-G*$^{+/-}$ mice (Figure 1d). The general appearance and behaviour of these mice was normal and they were indistinguishable from their wild-type (WT) littermates.

As expected, no RNA could be detected by RT-PCR in tissues from *Bcl-G*$^{-/-}$ mice (Figure 2a). Our mAb (clone 2E11) detected a 38-kDa band in WT testis, and this band was absent from *Bcl-G*$^{-/-}$ testis (Figure 2b). Interestingly, only one Bcl-G isoform is produced from the mouse *Bcl-G* gene, whereas a long (BCL-G_L) and a short (BCL-G_S) isoform are produced from human *BCL-G*.[4] In the testis, Bcl-G immunoreactivity was limited to the late-stage spermatids within the seminiferous tubules (Figure 2c). No staining was seen in the mature sperm found in the epididymal tubules (data not shown). Interestingly, Bcl-G-deficient male (and female) mice exhibited normal reproductive behaviour and produced litters of normal size.

Bcl-G is expressed in diverse mouse tissues but is not required for their development and function. In addition to the male reproductive organs, high levels of mBcl-G were also found in the thymus, small intestine and colon. Intermediate expression levels were seen in pancreas, spleen and lung, whereas little or no Bcl-G expression was observed in the brain, kidney and liver (Figure 3a). Mouse Bcl-G protein is most similar to human BCL-G_L, and its expression closely matches what is known for h*BCL-G*$_L$ mRNA.[4]

Bcl-G expression was high in many epithelial cells, in particular those lining the gastrointestinal tract and the lumen of mammary ducts (Figure 3b and data not shown). However, no obvious defects were found in these organs in *Bcl-G*$^{-/-}$ mice. *Bcl-G*$^{-/-}$ intestines had similar lengths of villi and crypt depths as those from WT mice (Figure 3b). The numbers of Paneth and goblet cells were also normal, indicating that Bcl-G is not required for intestinal epithelial differentiation (data not shown). In the mammary gland, Bcl-G loss did not affect ductal morphogenesis, and the lumens of ducts in *Bcl-G*$^{-/-}$ females were clear and well developed (Figure 3b). As the survival and growth of pups from litters of *Bcl-G*$^{-/-}$ females was no different from those of WT mothers, we conclude that Bcl-G deficiency did not significantly affect mammary development during pregnancy, nor did it affect milk production or nursing behaviour (data not shown).

Bcl-G is expressed by dendritic cells. Bcl-G was expressed in large cells within the thymic medulla and the centre of lymphocytic follicles of the spleen and lymph nodes (Figure 3b, and data not shown). No significant Bcl-G staining was detected in lymphocytes. The Immunological Genome Project gene expression database revealed high expression of *Bcl-G* mRNA in CD8$^+$ dendritic cells (DCs).[6] We examined Bcl-G expression in select DC subsets from WT spleen using our Bcl-G-specific antibodies (Figure 3c). In accordance with the mRNA expression results, conventional DCs (cDCs; CD11c^{hi} CD45RA$^-$) had significantly higher levels of Bcl-G than plasmacytoid DCs (pDCs; CD11c^{int} CD45RA$^+$) (Figure 3c). This high expression was largely contributed by the CD8$^+$ cDC subset, although Bcl-G was also present at lower levels in the CD4$^+$ and double negative cDC subsets (Figure 3c). Bcl-G expression was increased in splenic cDCs upon stimulation with CpG oligonucleotides, perhaps indicating a role for Bcl-G in the Toll-like receptor 9 signalling pathway (Figure 3c).

The thymic medulla contains epithelial cells that are present in close proximity to the thymic DCs. As Bcl-G displayed expression in certain epithelial cell types in other organs, we investigated whether it is present in medullary thymic epithelial cells. However, double immunofluorescence staining for Bcl-G and the medullary thymic epithelial cell marker keratin-5 on WT thymus sections did not show any colocalisation, demonstrating that the DCs must constitute the majority of the Bcl-G-expressing cells in the thymus (Supplementary Figure 1).

Bcl-G$^{-/-}$ mice have normal haematopoietic cell subset composition. To investigate the impact of Bcl-G loss on the haematopoietic compartment, we analysed the cellular composition of blood, thymus and spleen in adult Bcl-G-deficient mice (Figures 4a–c). Overall numbers of red blood cells, white blood cells and platelets were all normal in Bcl-G-deficient mice (Figure 4a and data not shown). Similarly, thymi and spleens of *Bcl-G*$^{-/-}$ mice had similar weights and total cellularities as those of WT mice (Supplementary Figure 2, and Figures 4b and c). *Bcl-G*$^{-/-}$ mice also had normal numbers of each of the major thymic and splenic subpopulations analysed, showing that loss of Bcl-G did not affect the development and homeostasis of the mouse haematopoietic system (Figures 4b and c).

Bcl-G is dispensable for splenic DC development and apoptosis. As Bcl-G is highly expressed in DCs, particularly the CD8$^+$ subtype, we next measured the numbers of the various splenic DC subsets in *Bcl-G*$^{-/-}$ mice using flow cytometry (Figure 4d and Supplementary Figure 3). The numbers of *Bcl-G*$^{-/-}$ DCs were comparable to those in WT mice (Figure 4d and Supplementary Figure 3). Because of the higher expression of Bcl-G in CD8$^+$ DCs relative to other DC subsets, we also examined the function of the *Bcl-G*$^{-/-}$ CD8$^+$ DCs, using several antigen cross-presentation assays (Supplementary Figure 4). However, neither the *in vivo* cross-presentation assay nor the CTL killing assay revealed any difference between the WT and Bcl-G-deficient DCs, indicating that Bcl-G may not be required for cross-presentation and naive T-cell activation (Supplementary Figure 4).

We next compared the survival of *Bcl-G*$^{-/-}$ and WT DCs in culture (Figure 4e). Splenic DCs from the three subsets (pDC, CD8$^+$ and CD8$^-$ cDC) were purified by FACS and placed in

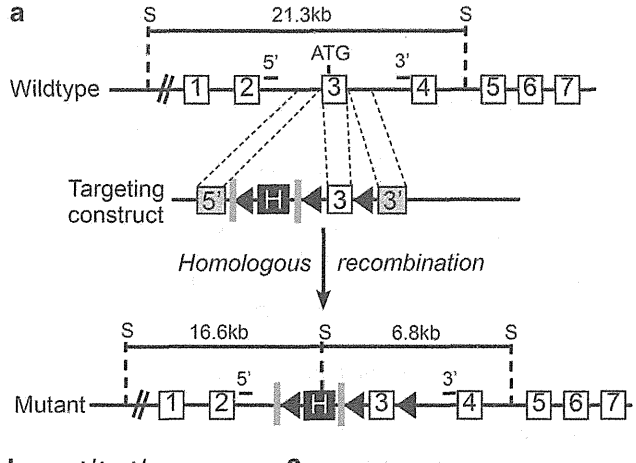

d

	% Offspring from crosses of *Bcl-G*$^{+/-}$ mice (#)		
	Bcl-G$^{+/+}$	*Bcl-G*$^{+/-}$	*Bcl-G*$^{-/-}$
Expected	25% (23)	50% (46)	25% (23)
Actual	37.1% (23)	40.3% (25)	22.6% (14)

Figure 1 Targeting strategy and generation of Bcl-G knock-out mice. (**a**) Schematic diagram depicting the *Bcl-G* locus targeting strategy. Open boxes represent exons and grey boxes represent intronic DNA (corresponding region on WT locus is indicated by dashed lines). H denotes the hygromycin resistance selection cassette (frt/loxP/pGK-Hygro/frt), whereas triangles and rectangles indicate the loxP sites and frt sites, respectively. The locations of the 5′- and 3′-external probes used for Southern blot analysis are shown. (**b**) Southern blot analysis on *Sca*I-digested genomic DNA to identify homologous recombination at the *Bcl-G* locus. Correctly targeted ES cell clones show a 16.6 kb fragment with the 5′-external probe and a 6.8 kb fragment with the 3′-external probe. (**c**) *Bcl-G*$^{-/-}$ mice were identified using a three-primer genotyping PCR protocol on tail DNA. Wild-type mice show a single band of 202 bp, whereas *Bcl-G*$^{-/-}$ mice show a single band of 346 bp. *Bcl-G*$^{+/-}$ mice show both bands. (**d**) Genotypes of offspring produced from crosses of *Bcl-G*$^{+/-}$ mice. The actual numbers are shown in brackets

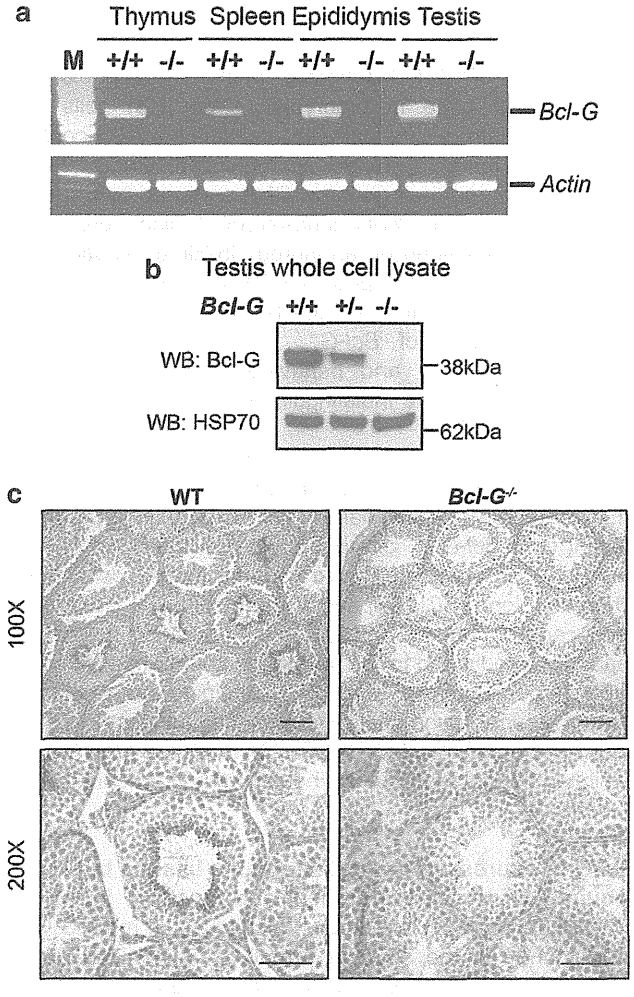

Figure 2 Loss of Bcl-G does not affect testicular development. (**a**) RT-PCR performed on mRNA using inter-exon primers confirmed the absence of functional *Bcl-G* transcripts in tissues of *Bcl-G*$^{-/-}$ mice. PCR using actin-specific primers served as a loading control. (**b**) Western blotting using Bcl-G-specific mAbs detected the presence of Bcl-G protein in testes of WT and *Bcl-G*$^{+/-}$ mice. No Bcl-G protein was detected in the testis from *Bcl-G*$^{-/-}$ mice. Membranes were reprobed for HSP70 as a loading control. (**c**) Anti-Bcl-G immunohistochemistry revealed that Bcl-G expression is limited to the late stage spermatids within the seminiferous tubules. Representative photomicrographs are shown at × 100 (bar represents 100 μm) and × 400 magnification (bar represents 40 μm)

medium with or without the survival factor granulocyte-macrophage colony-stimulating factor (GM-CSF; 10 ng/ml). Consistent with previous reports,[7,8] WT DCs, particularly the pDC subtype, underwent rapid cell death *in vitro*, with only ~20% pDCs surviving after 24 h in culture (Figure 4e). There was no significant difference in the rate of death of *Bcl-G*$^{-/-}$ DCs from any of the three subtypes when compared with their WT counterparts (Figure 4e). These results demonstrate that Bcl-G is not required for spontaneous DC apoptosis, both in the presence or absence of GM-CSF. Transient overexpression of mouse Bcl-G did not cause significant killing of 293T cells (Supplementary Figure 5A), further indicating that mBcl-G lacks significant pro-apoptotic activity.

Bcl-G does not bind strongly to the prosurvival Bcl-2-like proteins. The complex interactions between three major subgroups of the Bcl-2 family determine whether apoptosis is activated or not.[9,10] Human BCL-G_S was reported to bind BCL-X_L through its BH3 domain, whereas the presence of the additional BH2 domain in hBCL-G_L was suggested to prevent its binding to BCL-X_L.[4] As mBcl-G is most similar to hBCL-G_L, and as we could not find any evidence that mBcl-G exerted significant proapoptotic activity, we investigated whether it could even bind to the antiapoptotic Bcl-2 family members or Bax/Bak. Haemagglutinin (HA)-tagged mBcl-G was transiently overexpressed together with Flag-tagged prosurvival proteins (Bcl-2, Bcl-x_L, Bcl-w, Mcl-1 and A1), Flag-Bax, Flag-Bak or empty vector as a negative control (Figure 5a). Bcl-G could bind weakly to all

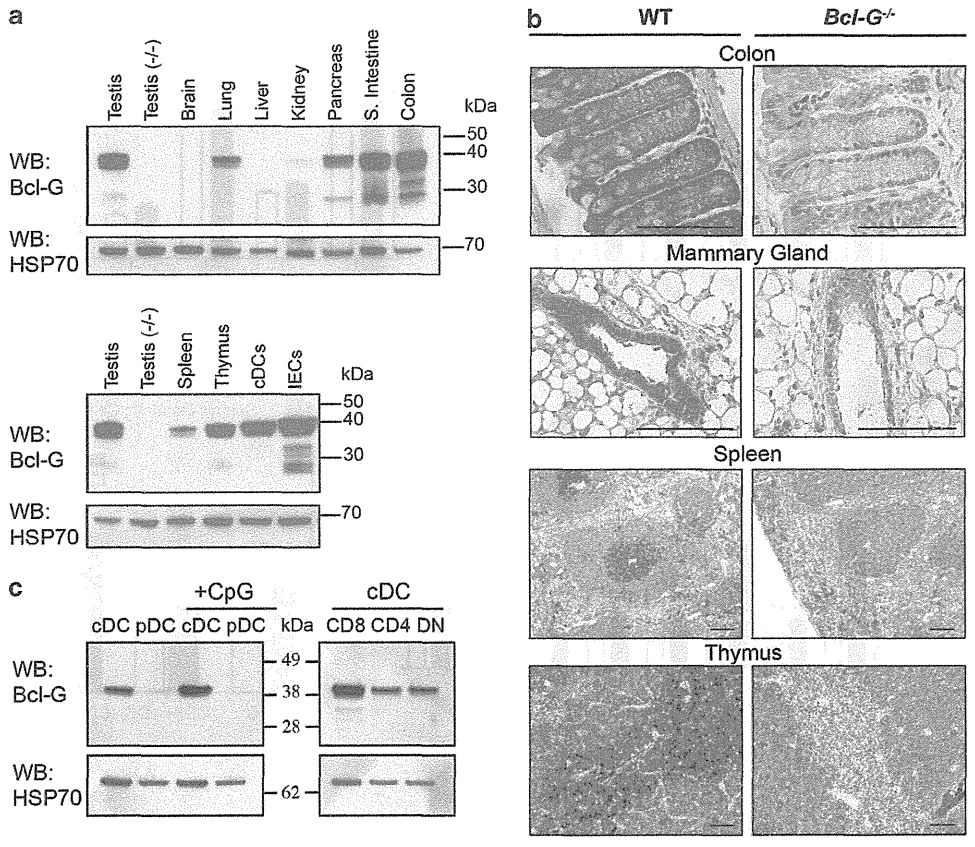

Figure 3 Bcl-G is expressed in eptihelial cells in a wide range of tissues and in DCs in the haematopoietic organs. (**a**) Western blot analysis of organs from C57BL/6 (WT) mice to determine distribution of Bcl-G. cDCs indicate FACS-sorted splenic conventional DCs ($CD11c^{hi}$ $CD45RA^{-}$), whereas IECs denote IECs isolated from WT intestines. Lysates from testis of *Bcl-G*$^{-/-}$ mice were used as a negative control. The membranes were reprobed for HSP70 as a loading control. (**b**) Immunohistochemistry using specific mAbs revealed cell type-specific expression of Bcl-G in the colon, mammary gland, spleen and thymus. Tissue sections from *Bcl-G*$^{-/-}$ mice were used as negative controls. The bars represent 100 μm. (**c**) Bcl-G expression in the various splenic DC subsets was analysed by western blotting. pDC stands for plasmacytoid DC ($CD11c^{int}$ $CD45RA^{+}$); CD8, CD4 and double negative (DN) indicates $CD8^{+}$ $CD4^{-}$, $CD8^{-}$ $CD4^{+}$ and $CD8^{-}$ $CD4^{-}$ cells, respectively). Bcl-G content in DCs stimulated with CpG DNA for 24 h was also analysed by western blotting

five prosurvival Bcl-2 family members when they were overexpressed (Figure 5a and Supplementary Figure 5B). In contrast, there was no evidence for significant interaction between mBcl-G and Bax or Bak (Figure 5a).

To determine the role of the BH3 domain in this weak binding, we generated several mutants of mBcl-G, including one lacking the entire BH3 domain (ΔBH3), one in which the conserved leucine within the BH3 domain was changed to alanine (L217A) and one which had the conserved glutamine and aspartate residues mutated to alanine (Figure 5b). Unexpectedly, these mutant Bcl-G proteins retained the ability to interact weakly with Bcl-x_L and all four other prosurvival proteins (Figure 5b and data not shown). These results indicate that Bcl-G might not bind to the prosurvival Bcl-2 family members in the same manner as the canonical BH3-only proteins, such as Bim or Puma. In accordance with what was reported for hBCL-G_L,[4] removal of the BH2 domain from mBcl-G increased its binding to Bcl-x_L (Figure 5b and Supplementary Figure 5B).

To further examine the ability of the BH3 domain of mBcl-G to bind to the prosurvival Bcl-2 family members, we generated a mutant form of Bim_S in which the BH3 domain was replaced with the BH3 domain of mBcl-G, and tested its binding to Bcl-x_L (Figure 5c). This experiment revealed that Bim_S(Bcl-G BH3), such as Bim_S(4E), a well-described non-Bcl-x_L-binding mutant of Bim_S,[11] did not bind Bcl-x_L (Figure 5c). This indicated that the BH3 domain of Bcl-G might be incapable of binding to the prosurvival Bcl-2 family members. Indeed, replacement of the BH3 domain of Bim with that of Bcl-G also resulted in complete loss of Bim's killing potential when overexpressed in 293T cells (Supplementary Figure 5A). Finally, we were unable to observe any endogenous binding of Bcl-G to Bcl-x_L, Bcl-2 and Mcl-1 in mouse tissue (testis, thymus or spleen) protein lysates when we immunoprecipitated either Bcl-G or Bcl-x_L (Supplementary Figure 6). Collectively, these observations suggest that Bcl-G might not function as a classical BH3-only protein.

Novel potential interacting partners for Bcl-G. We then conducted a proteomic screen to identify potential new interacting partners for Bcl-G and thus gain clues on a possible alternative function. The strategy is depicted in Figure 6. Whole-cell lysates were prepared from intestinal epithelial cells (IECs) isolated from WT or *Bcl-G*$^{-/-}$ mice. The presence of Bcl-G in the lysates from the WT cells but not in those from the control (*Bcl-G*$^{-/-}$) cells was verified by

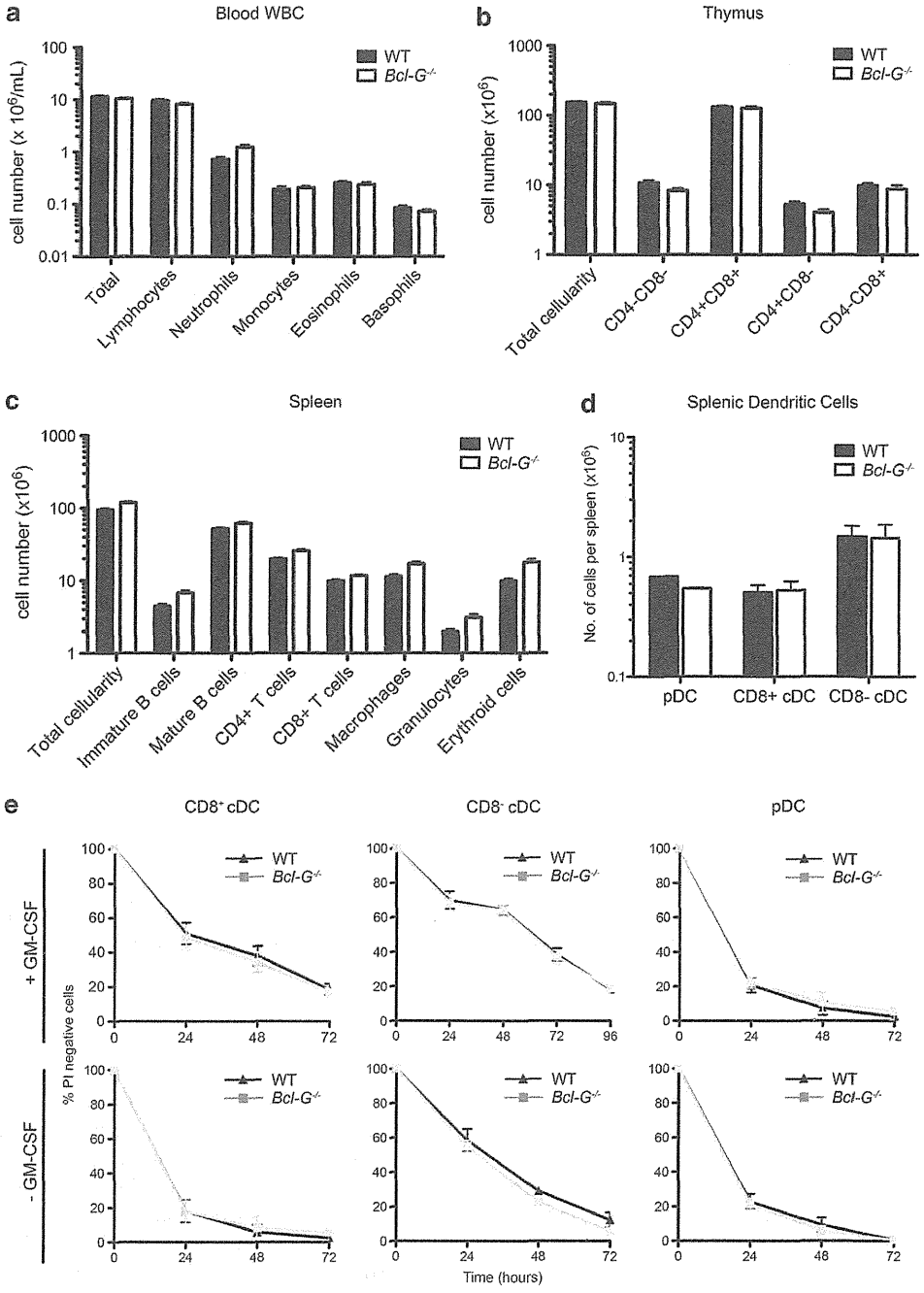

Figure 4 *Bcl-G*$^{-/-}$ mice have normal haematopoietic cell subset composition, and Bcl-G deficiency does not protect splenic DCs from apoptosis. (**a**) Leukocyte cell subset composition of 8–12-week-old WT and *Bcl-G*$^{-/-}$ mice was determined using an ADVIA blood analyser. Single-cell suspensions made from (**b**) thymi and (**c**) spleens of these mice were analysed by FACS after staining with antibodies against various cell surface markers to determine the numbers of the indicated cell subpopulations. Splenic subsets determined included B220^{+}sIgM^{hi}sIgD^{lo} immature B and B220^{+}sIgM^{lo}sIgD^{hi} mature B cells, Mac-1^{+}Gr-1^{-} macrophages, Mac-1^{+}Gr1^{+} granulocytes and Ter119^{+} nucleated erythroid cells. (**d**) Splenic DC subset composition was determined by flow cytometric analysis. The absolute numbers per spleen of cDC (CD11c^{hi}CD45RA^{-}), pDC (CD11c^{int}CD45RA^{+}), CD8^{+} cDC (gated cDC, CD8^{+}Sirpα^{-}) and CD8^{-} cDC (gated cDC, CD8^{-}Sirpα^{+}) are shown (see Supplementary Figure 3). (**e**) FACS-sorted splenic DC subpopulations from WT and *Bcl-G*$^{-/-}$ mice were plated into 96-well plates with or without addition of the DC survival promoting cytokine GM-CSF. Cell viability was determined at specific time points using propidium iodide staining followed by flow cytometric analysis. Data are presented as percentages of PI^{-} live cells *versus* time. The results shown represent at least three independent experiments ($n = 24$ of each genotype). Error bars indicate S.E.M.

western blotting (Supplementary Figure 7). Bcl-G protein complexes were immunoprecipitated from these protein lysates using two different Bcl-G-specific mAbs, 2E11 and 10C9, that recognise different epitopes within the Bcl-G protein (Figure 6). Immunoprecipitates were analysed by mass spectrometry.

A total of 327 unique proteins were identified in this screen (Figure 6). Of these, 216 proteins could be eliminated

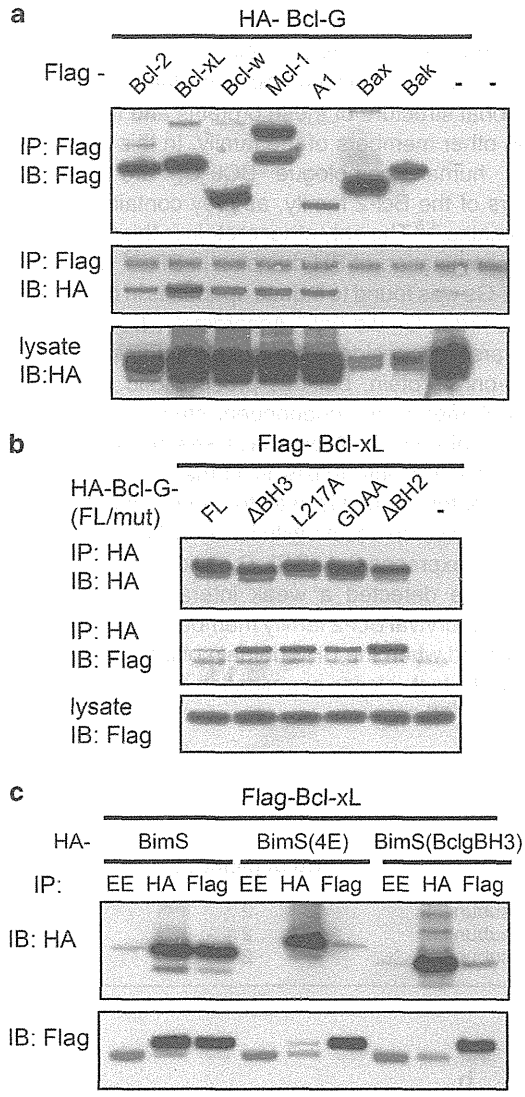

Figure 5 Weak interaction of Bcl-G with prosurvival Bcl-2 family members, which does not require its BH3 domain. Mammalian expression vectors encoding HA- and Flag-tagged proteins were co-transfected into 293T cells: (**a**) Full-length or (**b**) mutant HA-mBcl-G, together with Flag-tagged prosurvival proteins; (**c**) HA-mBim$_S$ (WT or mutant BH3) with Flag-Bcl-x$_L$. Empty HA and Flag vectors were used as negative controls (–). Immunoprecipitations were carried out using Protein G sepharose beads and antibodies against HA, Flag or Glu-glu (negative control). Immunoprecipitates were separated on SDS-PAGE gels and tested for the presence of co-immunoprecipitated Flag- or HA-tagged proteins by western blotting

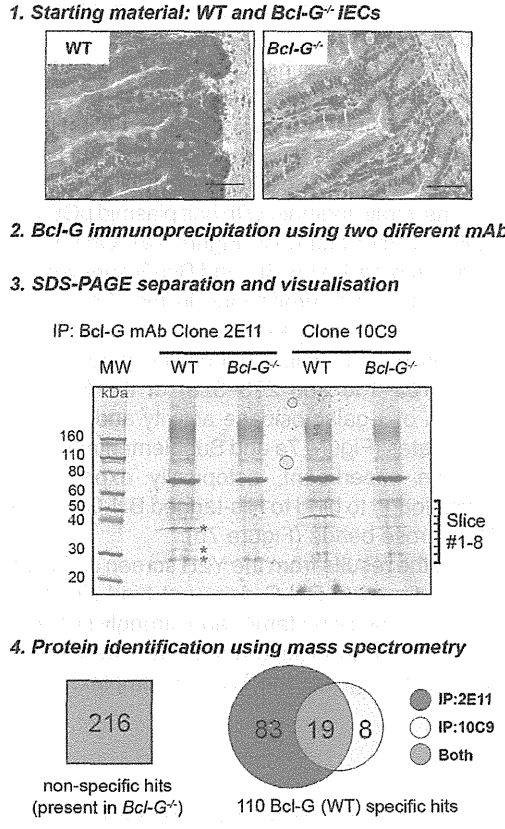

Figure 6 Identification of Bcl-G binding partners using IP–MS proteomic screening. Protein lysates made from IECs of WT or *Bcl-G*$^{-/-}$ mice (**1**) were used to immunoprecipitate Bcl-G using two independent anti-Bcl-G mAbs, 2E11 or 10C9 (**2**). Immunoprecipitated proteins were resolved by SDS-PAGE and visualised by Coomassie brilliant blue staining (**3**). Asterisks indicate the Bcl-G bands present in lane 1 (WT cell lysate, mAb 2E11) but not lane 2 (*Bcl-G*$^{-/-}$ cell lysate, mAb 2E11). Positions of molecular weight markers (MW) are shown. Corresponding regions for each sample were excised, trypsin-digested and sequenced by mass spectrometry (**4**). The 326 proteins identified in the screen were classified by their presence in each sample. Non-specific proteins were identified by their presence in either or both of the pull-downs from *Bcl-G*$^{-/-}$ cell lysates (216 proteins). Potential Bcl-G-interacting partners were identified as being present in either or both of the WT samples and absent in the *Bcl-G*$^{-/-}$ samples (110 proteins)

as non-specific interactors, as they were found in all the samples, including immunoprecipitates from *Bcl-G*$^{-/-}$ cells. As expected from the western blots, Bcl-G-derived peptides were only found in the WT samples (Supplementary Figure 8). A total of 110 unique proteins that potentially interact with Bcl-G were identified (Figure 6 and Supplementary Figure 9). Of these, 19 proteins were found in immunoprecipitates with both antibodies (Figure 6 and Supplementary Figure 9D). Notably, none of the Bcl-2 family members were identified in this screen, consistent with our overexpression/co-immunoprecipitation studies (Figure 5).

Yeast two-hybrid screening identifies Trappc6b as a Bcl-G-binding protein. We reasoned that an independent approach would help to validate and strengthen the results of the IP–MS experiment. We therefore used full-length Bcl-G as a bait to perform a yeast two-hybrid (Y2H) screening of a normalised mouse universal cDNA library (Clontech, Mountain View, CA, USA). In a screen of approximately 3×10^6 transformants, we obtained 52 colonies growing on plates containing selective medium. Of the cDNAs picked up in this screen, three were in the correct reading frame. cDNAs encoding the transport particle protein (TRAPP) complex 6b (Trappc6b) represented 19 of the 52 isolated clones. The other clones encoded parts of Sorting nexin 14 (Snx14) and Transmembrane protein 167B (Tmem167B) and were each found once. Importantly, none of the Bcl-2 family members were pulled down as potential Bcl-G-binding partners in this screen. In addition, mBcl-G did

not appear to bind to itself when overexpressed, in contrast to a previous report.[12]

Out of the three potential hits, we focused our attention on Trappc6b, as three components of TRAPP complexes (Trappc3, Trappc4 and Trappc5) had been identified in the IP–MS experiment (Table 1). To confirm the Y2H screening results, we introduced the pGADT7–Trappc6b plasmid into the AH109 yeast strain together with bait plasmid pGBT9–Bcl-G (FL) or pGBT9 vector alone (V; Figure 7a). Only yeast cells transformed with both Trappc6b, and Bcl-G survived on -Leu-Trp-His-Ade plates and turned blue in the X-gal assay that detects the presence of α-galactosidase activity (Figure 7a). This interaction was specific, as deleting particular regions (amino acids 103–136 and 273–328) of the Bcl-G protein resulted in lack of α-galactosidase activity and no growth on the selective plates (Figure 7a and Supplementary Figure 10). In a pull-down experiment, ectopically expressed Flag–Trappc6b was found to bind to His-tagged Bcl-G, immobilised on Ni-NTA agarose beads (Figure 7b).

Collectively, the results from the Y2H screen and the IP–MS experiment confirm that Bcl-G does not bind significantly to other members of the Bcl-2 family and strongly suggest that it is involved in vesicle trafficking and protein transport across the cells by interacting with the TRAPP complex.

Discussion

Proteins of the Bcl-2 family are characterised by the presence of BH domains that are important in determining the three-dimensional structure of these proteins and their interactions with the other members of the family. In this regard, mBcl-G and its human homologue BCL-G_L are rather unique members of the Bcl-2 family, as they contain both BH3 and BH2 domains.[4,5] The only other protein in this family to contain such a combination of BH domains is Bfk.[13] Overexpression of hBCL-Gs was found to induce apoptosis in certain cell lines, whereas hBCL-G_L did not.[4] Accordingly, *BCL-G* is widely (if not universally) considered to encode yet another proapoptotic BH3-only protein, but this proapoptotic activity has not been confirmed in an independent study, let alone within a physiological context. A database search indicated that the BCL-G_S isoform only exists in humans, as the alternative splice acceptor site that is used to produce it is not conserved in other species. In accord with its lack of killing activity (even when overexpressed), hBCL-G_L did not bind BCL-X_L.[4] Although we detected a weak interaction of mBcl-G with several prosurvival Bcl-2 family members, this interaction was still observed when the BH3 domain of Bcl-G was mutated or removed. In fact, closer examination indicates that the BH3

Table 1 Trapp complex subunits identified as potential mouse Bcl-G-binding partners in the IP–MS proteomic screen

Acc. no.	Gene symbol	Protein name	No of peptides	% Coverage
Q9ES56	*Trappc4*	Trafficking protein particle complex subunit 4	2	11.00
Q9CQA1	*Trappc5*	Trafficking protein particle complex subunit 5	2	9.57
O55013	*Trappc3*	Trafficking protein particle complex subunit 3	2	12.80

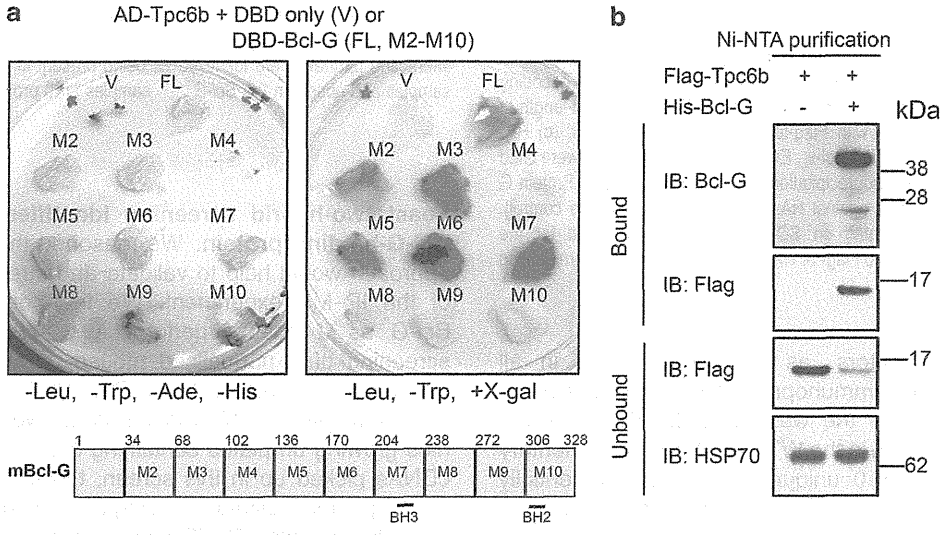

Figure 7 Trappc6b interacts with mBcl-G in the Y2H assay. (**a**) pGBT9-DBD empty vector or pGBT9-DBD-mBcl-G (full-length and truncation mutants M2–M10) were co-transformed with pGADT7-AD-Trappc6b into the yeast strain AH109. Positive interactions were tested by streaking transformants onto a -Leu-Trp-His-Ade plate (left) and the β-galactosidase assay was performed using X-gal staining of yeasts growing on a -Leu-Trp plate (right panel). The amino acid positions of the truncations within the Bcl-G mutants are shown in the schematic below. See Supplementary Figure 9 for more details. (**b**) Cell lysates made from 293T cells overexpressing Flag-Trappc6b were added to Ni-NTA beads pre-incubated with recombinant His-mBcl-G purified from *Escherichia coli*. Flag-Trappc6b bound to immobilised Bcl-G was identified by anti-Flag western blotting. Detection of unbound Trappc6b in the control sample indicates input. Probing for HSP70 served as a control that equal amounts of protein lysates were used

domain of Bcl-G does not conform to the BH3 consensus sequence; for example, the uniformly hydrophobic residue in position Φ3 is replaced with a serine (S220). This may explain why mBcl-G binds poorly to prosurvival family members. Strikingly, no Bcl-2 family member, prosurvival or proapoptotic, was pulled down in either our proteomic screen or the Y2H screen. Collectively, these results indicate that mBcl-G is most likely not involved in interactions with other Bcl-2 family members and, therefore, probably does not function in the intrinsic apoptotic pathway.

To determine which tissues and cell types normally express Bcl-G, we have generated three highly specific mAbs.[14] In western blots, mBcl-G appears as a ~38-kDa band that is not present in *Bcl-G*$^{-/-}$ animals. It is worth noting that some of the earliest commercially available anti-BCL-G antibodies detect a single ~22-kDa band that corresponds neither to the size of hBCL-G_L nor that of hBCL-G_S. We found that Bcl-G is highly expressed in many epithelial cells, as well as in DCs. This guided the choice of the source of protein lysates for our IP–MS experiment, as we wanted to avoid using Bcl-G overexpression. Our search for novel interacting partners using two independent approaches led to the discovery that Bcl-G may be a component of the TRAPP complex, which is involved in vesicle-mediated protein transport. Two large multi-subunit TRAPP complexes have been identified in yeast, whereas there seems to be only one TRAPP complex in mammals.[15] These complexes function in the endoplasmic reticulum (ER) to Golgi transport, as well as intra-Golgi transport. Our immunofluorescence studies did not reveal any specific subcellular localisation of Bcl-G in the Golgi, ER or within vesicular structures when overexpressed in HeLa cells.[14] However, Bcl-G overexpressed in HeLa cells may not reflect its physiological localisation as it was shown in the case of Trapp complex subunit 3.[16] As Bcl-G does not exist in yeast, it is difficult to predict what its precise function in the TRAPP complex is, and more work is required to determine this function.

The *BCL-G* gene is located on human chromosome region 12p12–13, which has been associated with a range of malignancies.[17] A search for a putative prostate cancer tumour suppressor gene within this region revealed that *Bcl-G* transcript levels were downregulated in tumour samples compared with normal prostate tissue.[18] No mutations or expression changes of the *Bcl-G* gene were found in children with acute lymphoblastic leukaemia,[17] but a TEL–AML1 fusion transcript involving *BCL-G* was reported in another.[19] In breast cancer, Bcl-G expression was found to be abnormally reduced and possibly regulated post-translationally by maternal embryonic leucine zipper kinase, a recently identified protein kinase and candidate oncoprotein upregulated in several types of cancer.[20] In all these studies, BCL-G was considered a proapoptotic BH3-only protein and, as such, a potential tumour suppressor. These considerations must now be revised in the light of our results, which show that Bcl-G is not an inducer of apoptosis, although they do not preclude by any means that BCL-G may still work as a tumour suppressor. Hence, the importance of Bcl-G in initiation and progression of cancer remains to be studied.

Certain cell types with prominent Bcl-G expression were studied in detail in an attempt to identify a defect caused by the loss of this protein. Most DCs have a short lifespan, and upon activation and antigen presentation, they rapidly undergo apoptosis to limit the potency of the immune response that had been elicited.[8,21] Members of the Bcl-2 protein family have critical roles in DC apoptosis.[21–23] For example, DCs from *Bim*$^{-/-}$ mice are abnormally resistant to spontaneous apoptosis, leading to enhanced T-cell activation and autoantibody production *in vivo*.[7,24] In contrast, loss of Bcl-G did not impact on DC lifespan, nor did it significantly impact on their main functions, such as antigen cross presentation.

The lack of an obvious phenotype in Bcl-G-deficient mice could be attributed to the existence of functional redundancy, as was reported for other members of the Bcl-2 protein family.[25] However, our results have indicated that Bcl-G might not have a proapoptotic function after all. It thus seems reasonable to investigate the function of Bcl-G further before embarking on time-consuming and costly double-knockout studies.

Several BH3 domain-containing proteins have been shown to function outside the conventional Bcl-2-regulated apoptotic pathway, including cell cycle control, autophagy, calcium homeostasis and ER morphogenesis.[3] It appears likely that Bcl-G may have to be added to this list. The Bcl-G-deficient mice as well as the mAbs that we have generated should prove valuable tools to further study this intriguing Bcl-2 family member.

Materials and Methods

Generation of Bcl-G$^{-/-}$ mice. The targeting construct was designed to introduce loxP sites on either side of the ATG start codon containing exon 3, as well as an FRT-flanked PGK-hygromycin resistance cassette for screening purposes. The targeting construct was electroporated into C57BL/6-derived Bruce-4 ES cells.[26] Homologous recombination events were identified by Southern blotting, using external 5′- and 3′-genomic probes, and blotting with a hygro-specific probe confirmed single-construct integration. Two correctly targeted ES cell clones were injected into blastocysts, resulting in two independent *Bcl-G* gene-targeted mouse strains. Exon 3 and the hygromycin-resistance cassette were deleted by crossing the resultant *Bcl-G*$^{loxP/wt}$ heterozygous mice with C57BL/6 cre deleter mice, and the Cre transgene was subsequently eliminated by crossing offspring to C57BL/6 mice. All of the mice analysed were devoid of hygro and cre. Genotyping of Bcl-G-deficient mice was performed using a three-primer PCR reaction using a common forward primer (5′-TCCGTCCCATTATAACCCTA-3′), together with two reverse primers (5′-CTGGAACGACAGAGGGCAAA-3′ and 5′-TACCATCACAGAGCCAGAA-3′). The WT and mutant alleles produced products of 202 and 346 bp, respectively.

C57BL/6, B6.CH-2*bm* 1 (*bm1*) and OT-I[27] mice were obtained from WEHI Bioservices (Kew, VIC, Australia). All animal procedures were reviewed and approved by the Melbourne Directorate Animal Ethics Committee.

RT-PCR analysis. RNA extraction was performed with the TRIzol method (Life Technologies, Mulgrave, VIC, Australia) according to the manufacturer's instructions. cDNA was synthesised using the TaqMan Gold RT-PCR kit (Life Technologies). The PCR amplification step used GoTaq Green Master Mix (Promega, Alexandria, NSW, Australia) and 25 pmol of each forward (5′-CCCAAGCTCTCCAGAACAAG-3′) and reverse (5′-CAGCAGCTCAACAATCTTGC-3′) primers.

Western blotting and immunoprecipitation. HEK293T cells were maintained in Dulbecco's modified Eagle's medium (DMEM) supplemented with 10% fetal bovine serum, transiently transfected using Fugene 6 reagent (Roche, Dee Why, NSW, Australia), and were harvested 40 h post-transfection. Cells were lysed in 20 mM Tris-pH 7.4, 135 mM NaCl, 1.5 mM MgCl2, 1 mM EGTA, 10% glycerol and 1% Triton X-100 supplemented with complete protease inhibitor cocktail tablets (Roche). Lysates were incubated with protein G-sepharose beads and antibodies against HA (3F10; Roche), Flag (M2; Sigma-Aldrich, Rowville,

VIC, Australia) or EE (Glu-Glu; Covance, North Ryde, NSW, Australia). Protein complexes were resolved on 4–12% Bis-Tris SDS-PAGE gels (Life Technologies) and detected on western blots with rat mAbs to Bcl-G (2E11)[14] or HA and mouse mAbs to Flag (M2, Sigma-Aldrich), HSP70 (N6; a kind gift from Dr R Anderson, Peter MacCallum Cancer Research Centre, Melbourne, VIC, Australia) or Actin (AC-40; Sigma-Aldrich). Labelled protein bands were detected by incubation with goat anti-mouse Ig or goat anti-rat IgG antibodies conjugated to horseradish peroxidase (Southern Biotech, Birmingham, AL, USA), followed by chemiluminescence analysis (ECL; GE Healthcare, Rydalmere, NSW, Australia)

Histology and tissue immunohistochemistry. Mouse tissues were fixed in 10% formalin. Protocols used for immunohistochemistry and immunofluorescence have been described.[14]

Immunofluorescence and flow cytometric analysis. Peripheral blood was analysed with the ADVIA 120 Hematology System (Bayer, Tarrytown, NY, USA). Single-cell suspensions prepared from thymi and spleens were counted using the CASY Cell Counter (Roche). Cells were stained for flow cytometric analysis using fluorochrome (fluorescein isothiocyanate, PE, APC or PerCP)-conjugated antibodies to Thy1.2 (T24.31.2), CD8 (YTS169), B220 (RA3-6B2), IgM (5.1), IgD (1126C), Gr-1 (8C5), CD3 (KT3-1.1), CD4 (YTA-321), CD11b (Mac-1) and Ter-119 (erythroid cell marker). Staining with propidium iodide (5 μg/ml) was used to label dead cells. Data were acquired on either a FACScan or an LSR II flow cytometer (BD Biosciences, San Jose, CA, USA). All data analysis was performed using FlowJo software (TreeStar, Ashland, OR, USA).

DC isolation and treatments. DCs were isolated from spleens of mice according to previously published protocols,[28] followed in some cases by high-speed cell sorting (MoFlo, Cytomation, Fort Collins, CO, USA). DC populations purified from WT or *Bcl-G*$^{-/-}$ mice were added to 96-well plates at 1×10^5 cells per well in RPMI medium 1640 supplemented with 10% FCS, 50 μM 2-mercaptoethanol, 2 mM L-glutamine, 100 units/ml penicillin, 100 μg/ml streptomycin with or without supplementation with 100 ng/ml GM-CSF (PeproTech, Rocky Hill, NJ, USA) and/or 0.5 μM CpG_{1168} (Geneworks, Hindmarsh SA, Australia). *In vivo* OT-I TCR transgenic T-cell proliferation assays and *in vivo* CTL assays were performed as described.[29]

Isolation of primary small IECs. Small intestines from either WT or *Bcl-G*$^{-/-}$ mice were removed, opened longitudinally, cut into 0.5-cm pieces and placed into ice-cold DMEM media containing 1 mM DTT. Gut pieces were shaken gently for 15 min at 37 °C, the dislodged cells filtered out and solid material placed in PBS solution containing 15 mM EDTA, followed by a further 10-min incubation with shaking at 37 °C. After vortexing to dislodge IECs, cell suspensions were passed through cell strainers (100 μm, BD Biosciences) and centrifuged at 4 °C at 300 × *g* for 5 min.

Mass spectrometry. Immunoprecipitates were resolved on a 4–12% Bis-Tris SDS-PAGE gel (Invitrogen, Grand Island, NY, USA) and visualised by staining with the Colloidal Blue Staining Kit (Invitrogen). The gel regions between 25–55 kDa were excised and divided into eight equal slices, which were then subjected to in-gel reduction, alkylation and tryptic digestion. Extracted peptides were injected and fractionated by nanoflow reverse-phase liquid chromatography on a nano LC system (1200 series; Agilent, Santa Clara, CA, USA). The nano HPLC was coupled online to an LTQ-Orbitrap mass spectrometer equipped with a nanoelectrospray ion source (Thermo Fisher Scientific, Scoresby, VIC, Australia) for automated MS/MS. For protein identification within gel samples, LC-MS/MS data were searched against a non-redundant protein decoy database comprising sequences from the latest version of LudwigNR (Mouse Species, Melbourne, VIC, Australia). Mass spectra peak lists were extracted using extract-msn as part of Bioworks 3.3.1 (Thermo Fisher Scientific) linked into Mascot Daemon (Matrix Science, London, UK). Peak lists for each nano-LC-MS/MS run were used to search MASCOT v2.2.04 search algorithm (Matrix Science) provided by the Australian Proteomics Computational Facility (www.apcf.edu.au).

Y2H assay. A pre-transformed normalised Matchmaker mouse universal cDNA library prepared with pGADT7-RecAB was purchased from Clontech and screened by the Matchmaker GAL4 Two-Hybrid System (Clontech) according to the manufacturer's protocol. Full-length *mBcl-G* cDNA fragment was amplified by PCR and cloned into pGBT9 (Clontech). The yeast *Saccharomyces cerevisiae* strain AH109 (maintained in YEPD medium), which secretes α-galactosidase under the control of the MEL1 region, was transformed with pGBT9-mBcl-G and grown on a medium lacking tryptophan. The clone including the bait plasmid was transformed with the library plasmids. The transformed yeast cells were grown on 2% agar plates of a dropout medium lacking tryptophan, leucine, histidine and adenine (-Leu-Trp-His-Ade). The resulting colonies grown on the drop-out plate were inoculated again on a new drop-out plate containing 20 μg/ml X-α-Gal (5-bromo-4-chloro-3-indolyl-α-*O*-galactopyranoside; Clontech) and incubated at 30 °C for 7 days. Yeast co-transformed with pGADT7 and pGBT9 empty vectors, or pGBT9-p53 and pGADT7-LgT were used, respectively, as negative and positive controls. Total DNA was prepared from all positive blue colonies and introduced into *E. coli* TOP10 competent cells (Invitrogen). The prey plasmids were recovered and sequenced.

Ni–NTA agarose purification. Forty-eight hours post-transfection, 293T cells were washed with PBS and resuspended in onyx lysis buffer. Ni–NTA agarose beads (20 μl) (Qiagen, Chadstone, VIC, Australia) pre-incubated for 1 h with recombinant His-Bcl-G protein (12 μg) were washed, added to cell extracts and rotated at 4 °C for 2 h. Precipitates were washed four times with lysis buffer and then boiled in 40 μl 2 × NuPAGE LDS buffer (Invitrogen) followed by SDS-PAGE analysis.

Data analysis. All graphing and statistical analyses were performed using the Prism v4.0 (GraphPad Software, San Diego, CA, USA).

Conflict of Interest

The authors declare no conflict of interest.

Acknowledgements. We thank M Robati for technical assistance; LA O'Reilly for sharing reagents and expertise; G Siciliano, J Coughlin, E Sutherland and S O'Connor for mouse care; J Corbin for automated blood analysis; B Helbert and C Young for genotyping; K Wycherley for mAb production; E Tsui, S Mihajlovic and their team for histological preparations; and H Patsiouras and E Kapp from the Joint Proteomics Laboratory for mass spectrometry analysis. This work was supported by the Australian NHMRC (Program Grant 461221, Independent Research Institutes Infrastructure Support Scheme Grant 361646, and a Career Development Award), the Leukemia and Lymphoma Society (Specialised Center of Research Grant 7015), and infrastructure support from the NHMRC (IRISS) and the Victorian State Government (OIS). M Giam was funded by University of Melbourne under the Endeavour IPRS scholarship programme. JD Mintern is the recipient of an NHMRC Career Development Award.

1. Giam M, Huang DC, Bouillet P. BH3-only proteins and their roles in programmed cell death. *Oncogene* 2008; **27**: S128–S136.
2. Hinds MG, Day CL. Regulation of apoptosis: uncovering the binding determinants. *Curr Opin Struct Biol* 2005; **15**: 690–699.
3. Lomonosova E, Chinnadurai G. BH3-only proteins in apoptosis and beyond: an overview. *Oncogene* 2008; **27**: S2–S19.
4. Guo B, Godzik A, Reed JC. Bcl-G, a novel pro-apoptotic member of the Bcl-2 family. *J Biol Chem* 2001; **276**: 2780–2785.
5. Nakamura M, Tanigawa Y. Characterization of ubiquitin-like polypeptide acceptor protein, a novel pro-apoptotic member of the Bcl2 family. *Eur J Biochem* 2003; **270**: 4052–4058.
6. Heng TS, Painter MW. The Immunological Genome Project: networks of gene expression in immune cells. *Nat Immunol* 2008; **9**: 1091–1094.
7. Chen M, Huang L, Wang J. Deficiency of Bim in dendritic cells contributes to overactivation of lymphocytes and autoimmunity. *Blood* 2007; **109**: 4360–4367.
8. Chen M, Huang L, Shabier Z, Wang J. Regulation of the lifespan in dendritic cell subsets. *Mol Immunol* 2007; **44**: 2558–2565.
9. Youle RJ, Strasser A. The BCL-2 protein family: opposing activities that mediate cell death. *Nat Rev Mol Cell Biol* 2008; **9**: 47–59.
10. Strasser A, Cory S, Adams JM. Deciphering the rules of programmed cell death to improve therapy of cancer and other diseases. *EMBO J* 2011; **30**: 3667–3683.
11. Chen L, Willis SN, Wei A, Smith BJ, Fletcher JI, Hinds MG *et al.* Differential targeting of pro-survival Bcl-2 proteins by their BH3-only ligands allows complementary apoptotic function. *Mol Cell* 2005; **17**: 393–403.
12. Liu X, Pan Z, Zhang L, Sun Q, Wan J, Tian C *et al.* JAB1 accelerates mitochondrial apoptosis by interaction with proapoptotic BclGs. *Cell Signal* 2008; **20**: 230–240.
13. Coultas L, Pellegrini M, Visvader JE, Lindeman GJ, Chen L, Adams JM *et al.* Bfk: a novel weakly proapoptotic member of the Bcl-2 protein family with a BH3 and a BH2 region. *Cell Death Differ* 2003; **10**: 185–192.

14. Giam M, Mintern JD, Rautureau GJP, Hinds MG, Strasser A, Bouillet P. Detection of Bcl-2 family member Bcl-G in mouse tissues using new monoclonal antibodies. *Cell Death and Disease* 2012; **3**: e-pub ahead of print 23 August 2012; doi:10.1038/cddis.2012.117.
15. Sacher M, Kim YG, Lavie A, Oh BH, Segev N. The TRAPP complex: insights into its architecture and function. *Traffic* 2008; **9**: 2032–2042.
16. Yu S, Satoh A, Pypaert M, Mullen K, Hay JC, Ferro-Novick S. mBet3p is required for homotypic COPII vesicle tethering in mammalian cells. *J Cell Biol* 2006; **174**: 359–368.
17. Montpetit A, Larose J, Boily G, Langlois S, Trudel N, Sinnett D. Mutational and expression analysis of the chromosome 12p candidate tumor suppressor genes in pre-B acute lymphoblastic leukemia. *Leukemia* 2004; **18**: 1499–1504.
18. Latil A, Bieche I, Chene L, Laurendeau I, Berthon P, Cussenot O *et al.* Gene expression profiling in clinically localized prostate cancer: a four-gene expression model predicts clinical behavior. *Clin Cancer Res* 2003; **9**: 5477–5485.
19. Abdelhaleem M, Yi Q, Beimnet K, Hitzler J. A novel TEL-AML1 fusion transcript involving the pro-apoptotic gene BCL-G in pediatric precursor B acute lymphoblastic leukemia. *Leukemia* 2006; **20**: 1294.
20. Lin ML, Park JH, Nishidate T, Nakamura Y, Katagiri T. Involvement of maternal embryonic leucine zipper kinase (MELK) in mammary carcinogenesis through interaction with Bcl-G, a pro-apoptotic member of the Bcl-2 family. *Breast Cancer Res* 2007; **9**: R17.
21. Kamath AT, Henri S, Battye F, Tough DF, Shortman K. Developmental kinetics and lifespan of dendritic cells in mouse lymphoid organs. *Blood* 2002; **100**: 1734–1741.
22. Nopora A, Brocker T. Bcl-2 controls dendritic cell longevity *in vivo*. *J Immunol* 2002; **169**: 3006–3014.
23. Hon H, Rucker EB III, Hennighausen L, Jacob J. bcl-xL is critical for dendritic cell survival *in vivo*. *J Immunol* 2004; **173**: 4425–4432.
24. Fuertes Marraco SA, Scott CL, Bouillet P, Ives A, Masina S, Vremec D *et al.* Type I interferon drives dendritic cell apoptosis via multiple BH3-only proteins following activation by PolyIC *in vivo*. *PLoS One* 2011; **6**: e20189.
25. Coultas L, Bouillet P, Loveland KL, Meachem S, Perlman H, Adams JM *et al.* Concomitant loss of proapoptotic BH3-only Bcl-2 antagonists Bik and Bim arrests spermatogenesis. *Embo J* 2005; **24**: 3963–3973.
26. Lemckert FA, Sedgwick JD, Korner H. Gene targeting in C57BL/6 ES cells. Successful germ line transmission using recipient BALB/c blastocysts developmentally matured *in vitro*. *Nucleic Acids Res* 1997; **25**: 917–918.
27. Hogquist KA, Jameson SC, Heath WR, Howard JL, Bevan MJ, Carbone FR. T cell receptor antagonist peptides induce positive selection. *Cell* 1994; **76**: 17–27.
28. Vremec D, Pooley J, Hochrein H, Wu L, Shortman K. CD4 and CD8 expression by dendritic cell subtypes in mouse thymus and spleen. *J Immunol* 2000; **164**: 2978–2986.
29. Wilson NS, Behrens GM, Lundie RJ, Smith CM, Waithman J, Young L *et al.* Systemic activation of dendritic cells by Toll-like receptor ligands or malaria infection impairs cross-presentation and antiviral immunity. *Nat Immunol* 2006; **7**: 165–172.

Supplementary information accompanies the paper on Cell Death and Disease website (http://www.nature.com/cddis)

JVI
Journals.ASM.org

Sheeppox Virus SPPV14 Encodes a Bcl-2-Like Cell Death Inhibitor That Counters a Distinct Set of Mammalian Proapoptotic Proteins

Toru Okamoto,[a,b]* Stephanie Campbell,[c] Ninad Mehta,[c] John Thibault,[c] Peter M. Colman,[a,b] Michele Barry,[c] David C. S. Huang,[a,b] and Marc Kvansakul[a]*

The Walter and Eliza Hall Institute of Medical Research, Parkville, Victoria, Australia[a]; Department of Medical Biology, University of Melbourne, Parkville, Victoria, Australia[b]; and Li Ka Shing Institute for Virology, Department of Medical Microbiology and Immunology, University of Alberta, Edmonton, Alberta, Canada[c]

Many viruses express inhibitors of programmed cell death (apoptosis), thereby countering host defenses that would otherwise rapidly clear infected cells. To counter this, viruses such as adenoviruses and herpesviruses express recognizable homologs of the mammalian prosurvival protein Bcl-2. In contrast, the majority of poxviruses lack viral Bcl-2 (vBcl-2) homologs that are readily identified by sequence similarities. One such virus, myxoma virus, which is the causative agent of myxomatosis, expresses a virulence factor that is a potent inhibitor of apoptosis. In spite of the scant sequence similarity to Bcl-2, myxoma virus M11L adopts an almost identical 3-dimensional fold. We used M11L as bait in a sequence similarity search for other Bcl-2-like proteins and identified six putative vBcl-2 proteins from poxviruses. Some are potent inhibitors of apoptosis, in particular sheeppox virus SPPV14, which inhibited cell death induced by multiple agents. Importantly, SPPV14 compensated for the loss of antiapoptotic F1L in vaccinia virus and acts to directly counter the cell death mediators Bax and Bak. SPPV14 also engages a unique subset of the death-promoting BH3-only ligands, including Bim, Puma, Bmf, and Hrk. This suggests that SPPV14 may have been selected for specific biological roles as a virulence factor for sheeppox virus.

Viruses employ diverse strategies to subvert the death of infected host cells by apoptosis (23). The process of determining whether a cell lives or dies is critically dependent on the actions of Bcl-2 protein family members, which are key regulators of the mitochondrial or intrinsic pathway of apoptosis (68). Their central role is reinforced by the realization that certain viruses express sequence, structural, or functional homologs of mammalian Bcl-2 (13). Such members of the wider Bcl-2 family are readily recognizable, as they share one to four regions of sequence similarity, the *B*cl-2 *h*omology (BH) domains. In higher organisms, the prosurvival family members, such as Bcl-2, Bcl-x_L, and Mcl-1, keep cells viable unless they are bound and inactivated by the proapoptotic BH3-only proteins, such as Bim or Bad (44). BH3-only proteins are activated by damage signals triggered after cellular insults, such as growth factor deprivation or exposure to cytotoxic drugs, to initiate the cell death machinery (55). Unlike the prosurvival Bcl-2 proteins, which contain multiple BH domains, the BH3-only proteins contain only an α-helical BH3 domain, which binds a receptor-like groove on the prosurvival proteins (44). The key consequence is to activate the multidomain death mediators Bax and Bak to drive mitochondrial outer membrane permeabilization (MOMP), which results ultimately in the activation of proteolytic enzymes (caspases) that drive cellular demolition (27).

A number of viruses, including adenovirus (66), Kaposi sarcoma-associated herpesvirus (KSHV) (52), Epstein-Barr virus (EBV) (30), fowlpox virus FPV039 (1), and orf virus ORFV125 (64, 65), encode recognizable homologous Bcl-2-like proteins that were recognized by their sequence similarities indicating the presence of one or more BH domains (13). Subsequent structure determination of KSHV Bcl-2 (35) and EBV BHRF1 (36, 41) confirmed that both adopt the classical Bcl-2 fold encompassing the canonical hydrophobic binding groove observed in their cellular counterparts. Notably, viral Bcl-2-like proteins are often required for successful viral propagation, emphasizing the critical role inhibition of host cell apoptosis plays during viral infections (23). However, other viruses express antiapoptotic proteins that appear unrelated by sequence to known cell death regulators. They include myxoma virus-encoded M11L (19, 20, 25), human cytomegalovirus-encoded vMIA (24), murine cytomegalovirus-encoded m38 (38), and vaccinia virus-encoded F1L (21, 48, 49, 61, 63) and N1L (2, 7, 12). Despite the lack of sequence similarity to the Bcl-2 protein family, both F1L and M11L adopt a Bcl-2 fold (16, 40, 42), and the structure of M11L in complex with the BH3 peptide from Bak revealed that M11L binds BH3 ligands via the canonical BH3 binding groove (40). Similar to mammalian cell death antagonists, M11L acts to directly counter the cell death mediators Bax and Bak expressed by the host (40).

Overall, these studies suggest that there may be other yet-to-be-identified viral Bcl-2 proteins, and we embarked on a search for other viral gene products that bear sequence similarity to M11L to sample a different region of sequence space compared to cellular Bcl-2 proteins. Six candidate poxvirus genes were identified using a BLAST search, and one originating from sheeppox virus was selected for further analysis, since it appeared to be as potent an inhibitor of apoptosis as M11L in an initial cell death assay. Sheeppox virus is a member of the genus *Capripoxvirus* within the subfamily *Chordopoxvirus* of the *Poxviridae*. Sheeppox is endemic in

Received 4 May 2012 **Accepted** 24 July 2012
Published ahead of print 15 August 2012
Address correspondence to David C. S. Huang, huang_d@wehi.edu.au, or Marc Kvansakul, m.kvansakul@latrobe.edu.au.
* Present address: Marc Kvansakul, Department of Biochemistry, La Trobe University, Victoria, Australia; Toru Okamoto, Department of Molecular Virology, Research Institute for Microbial Diseases, Osaka University, Osaka, Japan.
Supplemental material for this article may be found at http://jvi.asm.org/.

doi:10.1128/JVI.01115-12

A

Accession No: virus: gene	Bcl-x_L	M11L	DPV84 gp022	SPV12	gp011L	DPV83 gp022	LD17	SPPV14
AAA46628: Myxoma virus: M11L	12.8	***	22.7	24.5	72.6	22.7	22.1	22.1
ABI99009.1: Deerpox virus: DPV84gp022	11.4	22.7	***	28.5	20.8	98.3	31.6	32.2
NP_570172.1: Swinepox virus: SPV12	12.0	24.5	28.5	***	28.2	28.5	31.7	32.3
NP_051900.1: Shope (Rabbit) fibroma virus: gp011L	12.1	72.6	20.8	28.2	***	19.6	21.2	21.2
YP_227399.1: Deerpox virus: DPV83gp022	10.8	22.7	98.3	28.5	19.6	***	31.6	32.2
AAN02583.1: Lumpy skin disease virus: LD17	12.8	22.1	31.6	31.7	21.2	31.6	***	94.4
NP_659590.1: Sheeppox virus: SPPV14	12.2	22.1	32.2	32.3	21.2	32.2	94.4	***

B

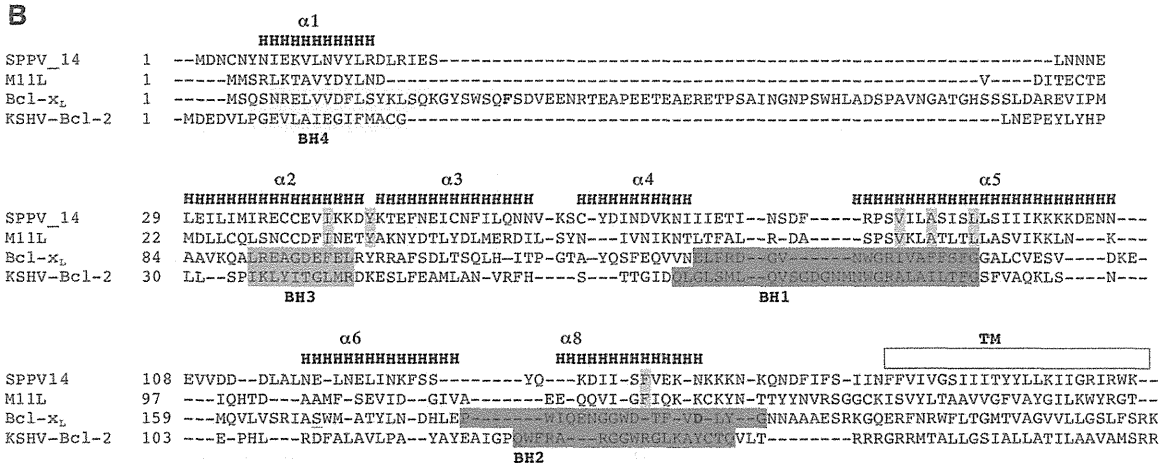

FIG 1 Identifying putative viral Bcl-2 (vBcl-2) homologs. (A) Using myxoma virus M11L as the query sequence in a BLASTP search of the NCBI database, six putative Bcl-2 family proteins encoded by viruses were identified (40). The pairwise identities (percent) in the amino acid sequences between the proteins were determined using ClustalW (57). Note the low sequence homology (<15%) of all the putative vBcl-2 proteins to human Bcl-x_L. (B) The amino acid sequence of a vBcl-2, SPPV14, was structurally aligned with those of myxoma virus M11L (40), mouse Bcl-x_L (44), and KSHV Bcl-2 (35). Based on this alignment, the residues making up α-helices 1 to 8 are marked "H." The colored shading indicates the BH1 (magenta), BH2 (orange), BH3 (green), and BH4 (yellow) Bcl-2 homology regions in Bcl-x_L and KSHV Bcl-2. The residues marked in cyan are those in the BH3 binding groove of M11L and conserved between it and SPPV14 (Fig. 2A). TM indicates the putative transmembrane region as taken from M11L.

Southwest and Central Asia, India, and North Africa and is a significant economic factor due to high mortality rates (50 to 70%), particularly in young animals. In cellular assays, we showed that sheeppox virus SPPV14 potently protects against diverse apoptotic stimuli, and here, we also report studies to define the molecular mechanism of action, and in particular, how it compares with other related proteins, such as myxoma virus M11L. Even though SPPV14 directly inhibits Bax and Bak, similar to M11L, it also binds a unique subset of the BH3-only proteins, suggesting that it may be functionally selected for a specific biological role(s) during the sheeppox virus life cycle.

MATERIALS AND METHODS

Expression and retroviral constructs. The cDNAs of deerpox virus (DPV83gp022 and DPV84gp022), swinepox virus (SPV12), shope fibroma virus (gp011L), lumpy skin disease virus (LD17), and sheeppox virus (SPPV14) were synthesized (GeneScript) and verified by sequencing. All mammalian expression vectors for hemagglutinin (HA)-tagged BH3-only proteins, HA-Bax and HA-Bak, subcloned into pEF PGKhygro have been described previously (9, 34, 46, 67). Similar constructs, made by subcloning into pEF PGKpuro, were generated for all viral proteins. A retroviral expression construct (Bim_S2A) was generated by subcloning into pMIG (murine stem cell virus [*M*SCV]-internal ribosome entry site [*I*RES]-green fluorescent protein [GFP], where the GFP sequence is that of enhanced GFP [EGFP]), as previously described (9, 67). The GFP selection cassette was replaced with the hygromycin resistance gene (58) for the constructs expressing viral proteins. Yeast constructs were made by subcloning into the pGALL(TRP) vector, as previously described (22). All cDNAs were of human or viral origin.

Details of all oligonucleotides and constructs used are available on request.

Tissue culture, cell death induction, retroviral infections, and apoptosis assays. All cell lines except Jurkat cells (HEK293T immortalized human embryonal kidney cell line, Phoenix Ecotropic packaging cells [39], and mouse embryonic fibroblasts [MEFs]) were cultured in Dulbecco's modified Eagle's medium (DMEM) supplemented with 10% fetal calf serum (FCS) and in some cases with 250 mM L-asparagine and 50 mM 2-mercaptoethanol. HuTK$^-$-143B and Jurkat cells were obtained from ATCC and maintained as previously described (62). Jurkat cells overexpressing Bcl-2 were generated and cultured as previously described (6); Bak- and Bax-deficient Jurkat cells were a gift from H. Rabinowich (University of Pittsburgh School of Medicine, Pittsburgh, PA) (60).

All MEFs (9, 67) were generated from embryonic day 13 (E13) to E14.5 embryos and immortalized at passages 2 to 4 with simian virus 40 (SV40) large T antigen. All mice used were of C57BL/6 origin or had been backcrossed (>10 generations), and their genotypes were determined as previously described (details are available on request).

Cell death was induced with 10 to 40 μM etoposide, UV irradiation (100 J/m^2), cytosine arabinoside (AraC), ABT-737 (1 μM; Abbott) (47), or FasL (Alexis) or by retroviral infection. pMIG retroviral constructs

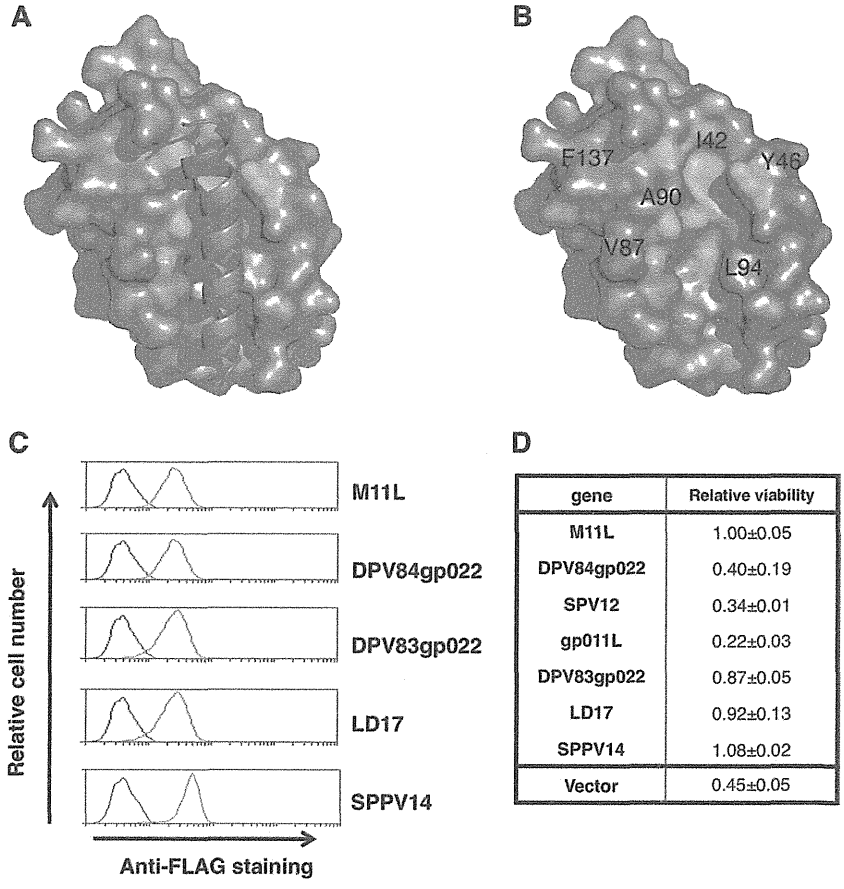

D

gene	Relative viability
M11L	1.00±0.05
DPV84gp022	0.40±0.19
SPV12	0.34±0.01
gp011L	0.22±0.03
DPV83gp022	0.87±0.05
LD17	0.92±0.13
SPPV14	1.08±0.02
Vector	0.45±0.05

FIG 2 Some putative vBcl-2 proteins block apoptosis. (A) Cartoon of the binding interface formed by the M11L-Bak complex (40). The M11L surface is shown in gray, and residues conserved between SPPV14 and M11L (Fig. 1B) that form part of the canonical binding groove in M11L are shaded in cyan. The Bak BH3 peptide is shown in orange. (B) Cartoon of the binding interface formed by the M11L-Bak complex. The colors are as in panel A, and the Bak BH3 peptide is removed for clarity. (C) The expression of FLAG-tagged viral proteins in MEFs was detected by flow cytometry. MEFs expressing novel vBcl-2 proteins were fixed and stained with an anti-FLAG antibody (red lines). The staining of MEFs expressing the empty vector is shown as the negative control (black lines). (D) The viability of MEFs expressing the empty vector, M11L, or poxvirus vBcl-2 proteins treated with etoposide (2.5 μM) for 24 h was determined by propidium iodide (PI) exclusion. The relative viability was determined by normalizing to that of M11L-expressing cells treated with etoposide. The data represent means ± standard deviations (SD) of two experiments performed with each cell line.

encoding BH3-only proteins were transiently transfected into Phoenix Ecotropic packaging cells, and viral supernatants were used to infect cells as described previously (9). Cell viability in both short-term assays and long-term assays of colony formation was determined as described previously (9). Long-term survival is expressed as a percentage of the number of colonies obtained relative to the number of colonies obtained after retroviral infection with empty parental retrovirus.

Bak activation was assessed by infecting 1×10^6 Jurkat cells, Jurkat cells expressing Bcl-2, or Bak- and Bax-deficient Jurkat cells at a multiplicity of infection (MOI) of 10 with VVEGFP (control wild-type vaccinia virus), VVΔF1L (F1L-deficient virus), or VVΔF1L-FLAG-SPPV14 (F1L-deficient virus expressing FLAG-tagged SPPV14). Six hours postinfection, the cells were fixed in 0.25% paraformaldehyde, permeabilized with 500 μg/ml (0.05%) digitonin (Sigma-Aldrich), and stained with a conformation-specific anti-Bak Ab-1 antibody (Oncogene Research Products) (28). Phycoerythrin-conjugated anti-mouse antibody was used to counterstain the cells (Jackson ImmunoResearch) before analysis by flow cytometry (FACScan; Becton Dickinson) using the FL-2 channel equipped with a 585-nm filter (42-nm band-pass). Data were analyzed using CellQuest software.

Protein production. The cDNA of SPPV14 was used to amplify the region coding for residues 1 to 145 of SPPV14 (deleting the C-terminal 31 amino acids, referred to as SPPV14ΔC31), which was cloned into the pET DUET vector (Invitrogen) using an introduced 5′ BamHI restriction site and 3′ EcoRI site, followed by a stop codon, and expressed in *Escherichia coli* BL21(DE3) pLysS cells. After homogenization in lysis buffer (20 mM Tris-HCl, pH 8.0, 150 mM NaCl, 10 mM 2-mercaptoethanol), the cell lysate was centrifuged and filtered prior to loading onto a 1-ml His-Trap column (Amersham). The protein was eluted in lysis buffer supplemented with 250 mM imidazole and subjected to gel filtration chromatography in 20 mM HEPES, pH 7.5, 150 mM NaCl, and 10 mM dithiothreitol (DTT) using a Superdex 200 column (Amersham), where it eluted as a single peak.

Immunoprecipitation and immunoblotting. The transfection and metabolic labeling of the human embryonic kidney (HEK293T cells with [^{35}S]methionine/[^{35}S]cysteine (NEN) have been described previously (33, 46). Immunoprecipitation of SPPV14 with Bak or Bax was performed using mouse monoclonal anti-FLAG (M2; Sigma) or anti-HA (HA11; Covance) antibody in buffer containing 20 mM Tris-HCl, pH 7.4, 135 mM NaCl, 1% Triton X-100, 10% glycerol in the presence of protease inhibitor (Roche). Control immunoprecipitations were performed using an anti-mouse Glu-Glu (MMS-115R; CRP) antibody. Proteins were resolved by SDS-PAGE (Novex gels; Invitrogen), transferred onto nitrocellulose membranes, and detected with X-ray film (Hyperfilm; GE Healthcare).

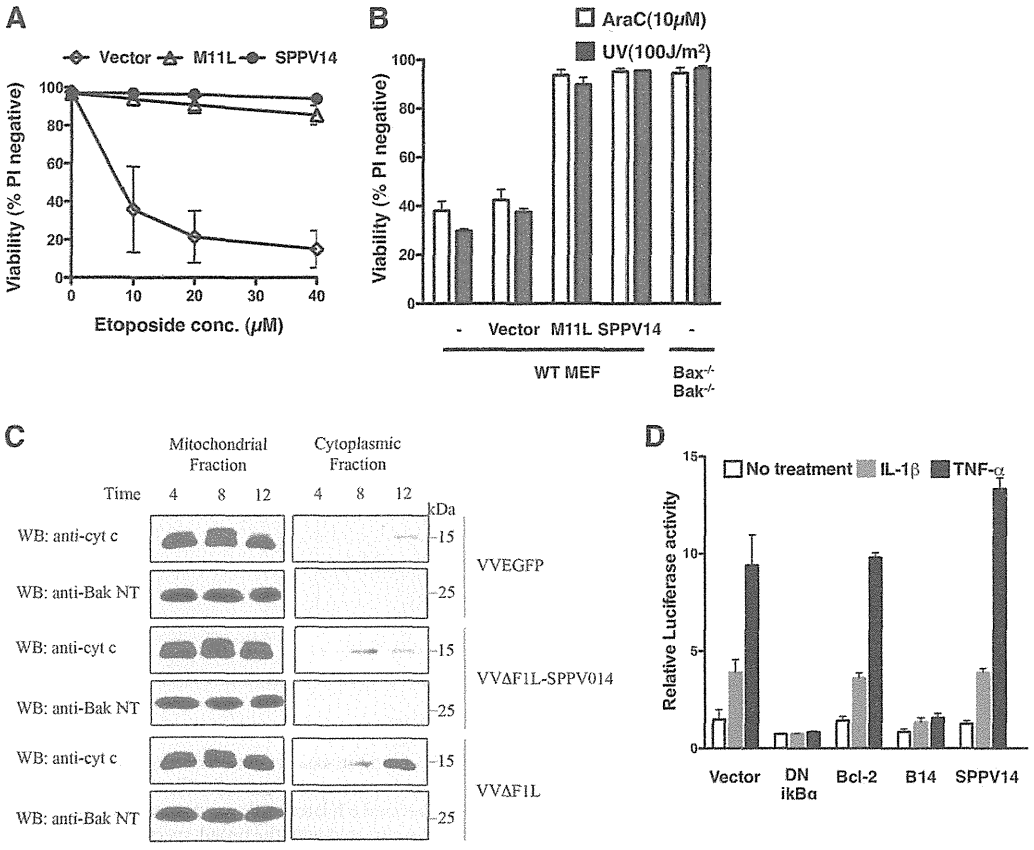

FIG 3 SPPV14 inhibits apoptosis, but not NF-κB activation. (A) Sheeppox virus SPPV14 is functionally comparable to myxoma virus M11L. Shown is the viability of wild-type (WT) MEFs expressing M11L or SPPV14, or the vector control, 24 h after treatment with 0 to 40 μM etoposide. (B) SPPV14 blocks apoptosis induced by diverse agents. Shown is the viability of MEFs (described in the legend to Fig. 1B) 24 h after treatment with 10 μM AraC or exposure to UV irradiation (100 J/m^2). The bars on the right show the viability of similarly treated Bax/Bak-doubly deficient MEFs. (C) SPPV14 prevents cytochrome *c* release. Jurkat cells were infected with VVEGFP, VVΔF1L-SPPV014, and VVΔF1L at an MOI of 10 for 4, 8, and 12 h. Mitochondrial pellets and cytoplasmic supernatants were separated via ultracentrifugation after treatment with digitonin. The mitochondrial pellets were resuspended in lysis buffer containing 0.1% Triton X-100, and 20% of the mitochondrial fractions and 50% of the cytoplasmic fractions were subjected to SDS-PAGE and immunoblotted with anti-cytochrome *c* and anti-Bak NT antibody as a control. WB, Western blotting. (D) SPPV14 does not block NF-κB activation induced by IL-1β or TNF-α. HEK293 cells were transiently transfected with an NF-κB luciferase reporter plasmid and the empty vector, dominant-negative (DN) IκBα, Bcl-2, B14, or SPPV14. The relative luciferase activity was measured 8 h after treatment with IL-1β (100 ng/ml) or TNF-α (100 ng/ml). The data represent means ± SD from 2 independent experiments.

Vaccinia virus production. SPPV14 cDNA was subcloned into pSC66, which places the gene under the control of a poxvirus promoter to generate VVΔF1L-FLAG-SPPV14 (17). Recombinant VVΔF1L-FLAG-SPPV14 was generated by homologous recombination of pSC66-FLAG-SPPV14 into the thymidine kinase locus of VVΔF1L, as described previously (17). In brief, 1 × 10^6 baby green monkey kidney (BGMK) cells were transfected with 5 μg of pSC66-Flag-SPPV14 and infected with VVΔF1L at an MOI of 0.05. Recombinant viruses were selected by growth on HuTK$^-$-143B cells in the presence of 5-bromodeoxyuridine (Sigma-Aldrich) and plaque purification using 5-bromo-4-chloro-3-indolyl-β-D-galactopyranoside (Rose Scientific Ltd.) to visualize β-galactosidase-positive viruses. All viruses were grown on BGMK cells.

Cytochrome *c* release. Jurkat cells (1 × 10^6) were infected with VVEGFP, VVΔF1L-SPPV014, and VVΔF1L at an MOI of 5 at 4, 8, and 12 h of infection. The cells were permeabilized in lysis buffer containing 75 mM NaCl, 1 mM NaH_2PO_4, 8 mM Na_2HPO_4, 250 mM sucrose, and 190 μg/ml of digitonin (Sigma-Aldrich), and the lysates were incubated on ice for 10 min (62). Mitochondrial and cytoplasmic fractions were separated by ultracentrifugation at 10,000 × *g* for 5 min. The mitochondrial pellet was resuspended in Triton X-100 lysis buffer containing 25 mM Tris, pH 8.0, and 0.1% Triton X-100 (Fisher Scientific). Samples were subjected to SDS-PAGE and immunoblotted with mouse anti-cytochrome *c* (BD PharMingen) and anti-Bak NT as a control.

PARP cleavage assay. To detect cleavage of poly-ADP ribose polymerase (PARP), Jurkat cells (1 × 10^6) were mock infected or infected with VVEGFP, VVΔF1L-SPPV014, and VVΔF1L at an MOI of 5. Cells were harvested 4, 8, 12, and 16 h postinfection and lysed in SDS-PAGE sample buffer containing 8 M urea. Samples were subjected to SDS-PAGE and immunoblotted with anti-PARP (BD PharMingen), anti-β-tubulin (EMC Bioscience), and anti-I3L to detect virus infection.

Solution competition assays. Solution competition assays using the Biacore optical biosensor were performed as described previously (9), using identical BH3 domain peptides and 10 nM SPPV14ΔC31.

Yeast colony assays. *Saccharomyces cerevisiae* W303α cells were cotransformed with pGALL(TRP) vector only, pGALL(TRP)-Bcl-x_L, or pGALL(TRP)-DPV022 and pGALL(Leu)-Bak or pGALL(Leu)-Bax. pGALL(TRP) and pGALL(Leu) place genes under the control of a galactose-inducible promoter (29). Cells were spotted as 5-fold serial dilutions onto medium containing 2% (wt/vol) galactose (inducing [ON]), which induces protein expression, or 2% (wt/vol) glucose (repressing [OFF]), which prevents protein expression, as previously described (37). Plates were incubated for 48 h at 30°C and then photographed.

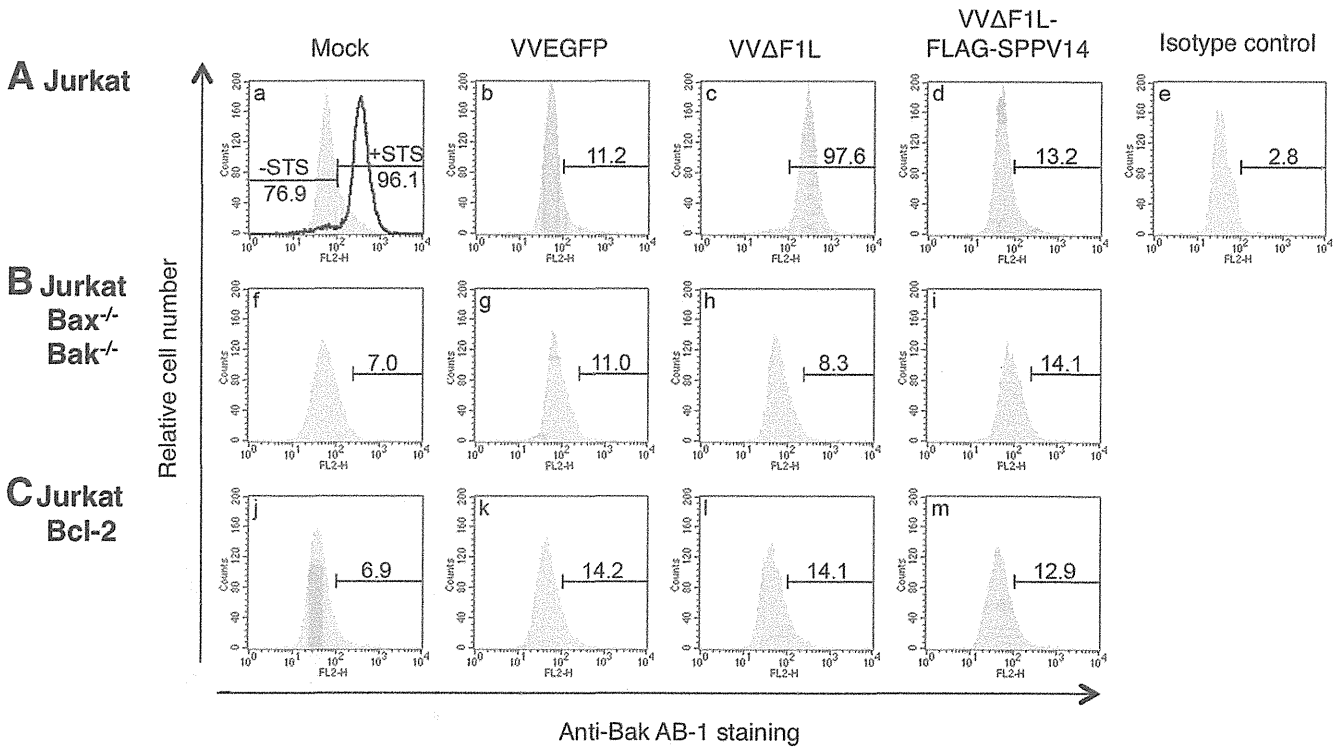

FIG 4 SPPV14 can functionally replace F1L during vaccinia virus infection. (A to C) SPPV14 inhibits Bak activation during vaccinia virus infection. Wild-type (A), Bax/Bak-doubly deficient (B), or Bcl-2-overexpressing (C) Jurkat cells were mock infected or infected with VVEGFP, VVΔF1L, or VVΔF1L-FLAG-SPPV14 (F1L-deficient virus expressing FLAG-tagged SPPV14) vaccinia virus. Bak activation was detected 6 h later by flow cytometric analyses of cells stained with the conformation-specific anti-Bak Ab-1 antibody (28). Positive-control mock-infected cells were treated with the broad-spectrum kinase inhibitor staurosporine (+STS) (A, a), known to induce apoptosis in many cell types. The bars mark the populations that contained activated Bak. Experiments were performed in triplicate. Fractions of Bak-activated cells are given as percentages.

RESULTS

Identifying putative viral Bcl-2 homologs. Although proteins such as Epstein-Barr virus BHRF1 (30) and adenovirus E1B19K (66) were first isolated due to their roles in modulating host-pathogen interactions during infection and in extending the life span of infected cells, they were later recognized as viral homologs of Bcl-2 (vBcl-2) by virtue of their sequence similarity to mammalian Bcl-2 (11). In contrast, herpesvirus saimiri-encoded ORF16 (54) and fowlpox virus-encoded FPV039 (1) were specifically recognized due to sequence similarity to mammalian Bcl-2. Aside from these readily identifiable viral Bcl-2-related proteins, the recent molecular and structural characterization of proteins such as M11L in myxoma virus (40, 59) and F1L in vaccinia virus (21, 42, 63), which appear to be unrelated to Bcl-2 by conventional sequence comparisons, has opened up another approach to identifying vBcl-2 proteins.

By searching for putative proteins that are related by sequence to M11L instead of mammalian Bcl-2, we circumvented the need for conventional genetic or functional screens in order to identify putative antiapoptotic factors encoded by other organisms. In a BLASTP search of the NCBI database (40), the top hits included six sequences that encode putative open reading frames (ORFs) from deerpox virus (DPV83gp022 and DPV84gp022), swinepox virus (SPV12), shope fibroma virus (gp011L), lumpy skin disease virus (LD17), and sheeppox virus (SPPV14) (Fig. 1A). Even though the overall sequence similarity to M11L was low, the critical residues forming the canonical binding groove in M11L (40) were conserved in all six proteins, strongly suggesting the presence of an analogous BH3 binding grove in these proteins (Fig. 1B and 2A and B).

To test if these ORFs encode antiapoptotic proteins, we expressed tagged versions of all six proteins in MEFs (Fig. 2C) and assessed their abilities to counter killing induced by the cytotoxic drug etoposide (Fig. 2D). DPV83gp022, LD17, and SPPV14 potently inhibited etoposide-induced killing, whereas DPV84gp022, swinepox virus (SPV12), and shope fibroma virus (gp011L) did not afford protection against etoposide, even though they were abundantly expressed. Interestingly, we noted that four residues (M52, T67, L68, and A71) in the binding groove of M11L are likely to be important for function, since the identified DPV84gp022, SPV12, and shope (rabbit) fibroma virus gp011L, which do not protect against apoptosis, have critical substitutions for these residues (see Fig. S1 in the supplemental material), possibly pointing to a biological function that does not involve apoptosis. We elected to focus further studies on SPPV14, since it was the most potent (Fig. 2D) out of all 6 identified putative vBcl-2 proteins and afforded protection against etoposide that appeared superior to that of M11L. Notably, SPPV14 shows 22% sequence identity to M11L. However, significantly higher conservation was apparent in the region corresponding to the central α5 helix that constitutes the BH1 region in M11L (10/21 amino acids; ~50%) (Fig. 1B).

Sheeppox virus SPPV14 is a potent inhibitor of mitochondrially mediated cell death. To extend the functional analysis, we examined the dose response following etoposide treatment.

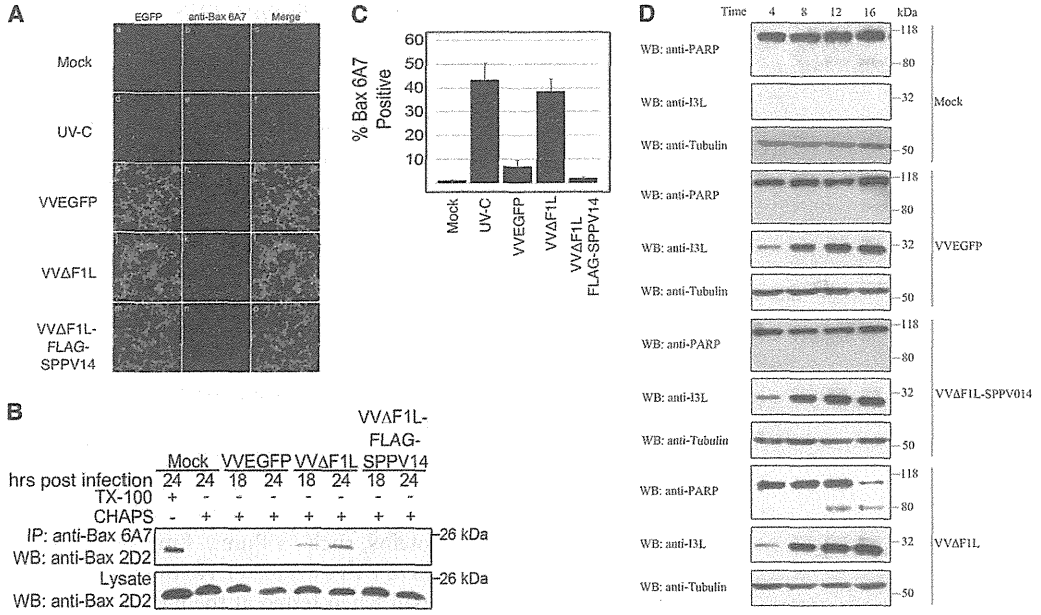

FIG 5 SPPV14 inhibits Bax activation during vaccinia virus infection. (A) HeLa cells were infected with VVEGFP, VVΔF1L, or VVΔF1L-FLAG-SPPV14 and incubated for 24 h. Infected cells or UV-C-irradiated HeLa cells were fixed and stained with the conformation-specific anti-Bax antibody 6A7, which specifically recognizes activated Bax (14, 31). (B) HeLa cells infected with VVEGFP, VVΔF1L, or VVΔF1L-FLAG-SPPV14 were lysed with Triton X-100 or CHAPS {3-[(3-cholamidopropyl)-dimethylammonio]-1-propanesulfonate}-based buffers and immunoprecipitated (IP) using the conformation-specific anti-Bax antibody 6A7. The immunoprecipitants were subjected to SDS-PAGE and blotted with the anti-Bax antibody 2D2, an antibody that recognizes all forms of Bax in immunoblots. (C) SPPV14 inhibits Bax activation induced by VVΔF1L. HeLa cells infected with VVEGFP, VVΔF1L, or VVΔF1L-FLAG-SPPV14 were incubated for 24 h and fixed, and Bax activation was measured by staining with anti-Bax 6A7 antibody (31) that specifically recognizes activated Bax. The data were quantified by counting 200 cells per experiment; means and SD of three replicate experiments are shown. UV-C, positive-control UV-irradiated HeLa cells. (D) SPPV14 inhibits PARP cleavage induced by VVΔF1L. Jurkat cells were mock infected or infected with VVEGFP, VVΔF1L-SPPV14, or VVΔF1L at an MOI of 5. Samples were collected 4, 8, 12, and 16 h postinfection, and the cells were lysed in SDS-PAGE sample buffer containing 8 M urea. Samples were subjected to SDS-PAGE and immunoblotted for PARP to determine the trigger of apoptosis; β-tubulin was used as a loading control and I3L as a sign of infection.

SPPV14 proved to be as efficacious as M11L (Fig. 3A), and its ability to counter killing induced by other agents, such as AraC or UV irradiation, was also comparable (Fig. 3B). Furthermore, SPPV14 appears to act at the mitochondrial checkpoint and not at the level of caspases, since it potently inhibits cytochrome *c* release (Fig. 3C).

As M11L was previously reported to protect against Fas-induced cell killing (59), we assessed the abilities of various virus-encoded antiapoptotic proteins to inhibit the extrinsic pathway of apoptosis. To induce CD95 (Fas) killing, FLAG-tagged Fas ligand was aggregated with the anti-FLAG antibody (32, 53). Notably, in cells treated with Fas ligand and cycloheximide, which is required for Fas-induced killing of MEFs, potent killing was observed (see Fig. S2 in the supplemental material). Expression of M11L, SPPV14, or vaccinia virus B14, a vaccinia virus virulence factor that inhibits IκB kinase (IKK) (26), had no impact upon Fas-induced killing (see Fig. S2). In MEFs, killing by Fas did not appear to be primarily regulated by the Bcl-2 protein family, since the loss of the essential death mediators Bax and Bak made little difference (see Fig. S2).

Having established that SPPV14 is a *bone fide* antiapoptotic protein (Fig. 2 and 3), we next determined if SPPV14 also interfered with NF-κB signaling, since some vBcl-2 proteins, such as vaccinia virus B14, A52, and N1L (2, 15, 26), fold like Bcl-2 but inhibit NF-κB. As expected, a dominant interfering mutant of IκBα effectively blocked activation of NF-κB induced by two cytokines, interleukin 1β (IL-1β) and tumor necrosis factor alpha (TNF-α), when HEK293T cells were cotransfected with a NF-κB reporter plasmid. Although we were able to confirm the ability of B14 to block NF-κB activation in this assay, neither Bcl-2 nor SPPV14 could (Fig. 3D), even though they were expressed. Overall, our results demonstrate that sheeppox virus SPPV14 can effectively inhibit multiple forms of apoptosis induced by the intrinsic (mitochondrial) pathway (Fig. 2 and 3) but does not appear to interfere with death through the extrinsic pathway or with NF-κB activation.

Sheeppox virus SPPV14 inhibits apoptosis during viral infection. Since SPPV14 can effectively inhibit killing triggered by experimentally applied stimuli, but not Fas, we next investigated its ability to inhibit apoptosis during viral infection (Fig. 4 and 5). Wild-type vaccinia virus infects and propagates in a wide range of mammalian cell lines, including Jurkat and HeLa cells. Deletion of the antiapoptotic protein F1L (63) from vaccinia virus results in apoptosis of infected cells, indicated by the activation of the key cell death mediators Bak (Fig. 4A) and Bax (Fig. 5). To determine if SPPV14 could functionally replace F1L and inhibit vaccinia virus-induced apoptosis, we inserted SPPV14 into a F1L-deficient vaccinia virus, and remarkably, SPPV14 was able to completely block Bak (Fig. 4A) and Bax (Fig. 5B and C) activation, thereby maintaining cell viability during infection with vaccinia virus. These findings are further supported by the observation that SPPV14 in the context of vaccinia virus infection also inhibits PARP cleavage (Fig. 5D).

In summary, we have demonstrated that sheeppox virus

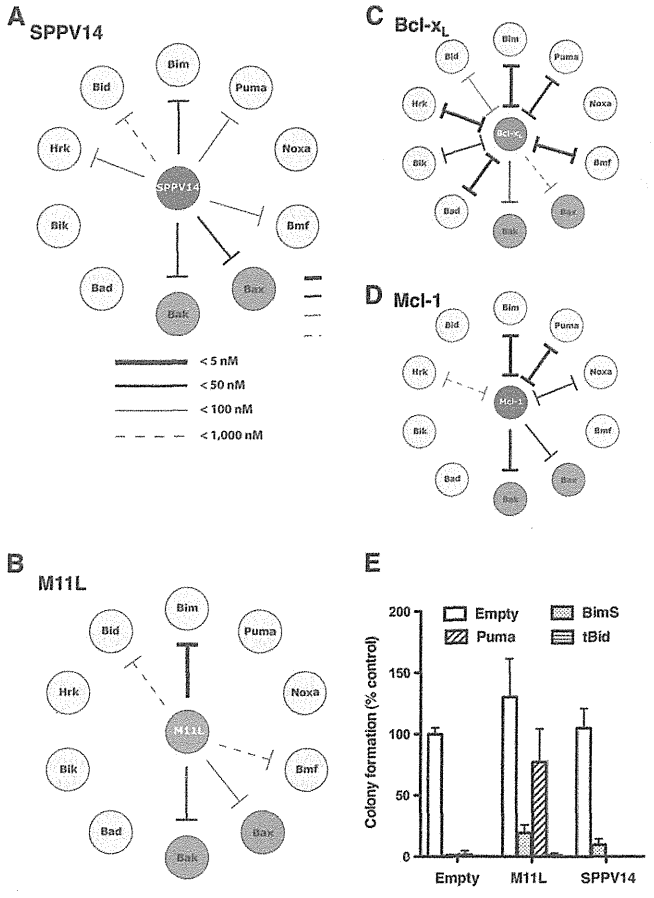

FIG 6 SPPV14 binds a unique set of mammalian proapoptotic proteins. (A to D) SPPV14 binds the BH3 domains of Bak, Bax, and certain BH3-only proteins. The relative binding affinities (IC_{50}) of recombinant SPPV14 (lacking its C terminus) for long BH3 peptides were determined by solution competition assays using the Biacore optical biosensor (9) (Table 1). The relative affinities of the interactions for SPPV14 (A), M11L (40) (B), Bcl-x_L (9) (C), and Mcl-1 (9) (D) are indicated by the thickness of the lines. Absence of a line indicates no binding. (E) Overexpression of Bim_S, Puma, and tBid counters the protection afforded by SPPV14. Shown is colony formation of M11L- or SPPV14-expressing MEFs infected with viruses expressing Bim_S, Puma, tBid, or an empty control. The number of colonies formed is expressed as a proportion of the colonies formed with the empty vector. The data represent means and SD from 2 independent experiments.

SPPV14 counters multiple experimentally applied inducers of apoptosis and appears fully functionally competent even in the context of infection with a distantly related virus, such as vaccinia virus.

SPPV14 interacts with a selective subset of mammalian Bcl-2 proteins. The capacity of most vBcl-2 proteins to inhibit apoptosis depends on the ability to bind and interfere with the action of mammalian proapoptotic proteins (4, 23, 40, 41, 61). Since SPPV14 potently prevented the activation of proapoptotic Bax and Bak (Fig. 4 and 5), we further investigated the molecular basis of Bax and Bak inhibition by testing the ability of SPPV14 to interact with mammalian proapoptotic Bcl-2 proteins. Initially, we evaluated the ability of recombinant SPPV14 to bind the BH3 domains of eight BH3-only proteins, as well as Bax and Bak, via solution competition assays (Fig. 6A and Table 1) (9). Bak and Bax BH3 domains were bound strongly with a 50% inhibitory concentration (IC_{50}) of <50 nM. For the BH3-only proteins, strong binding (IC_{50} < 50 nM) to Bim was observed, whereas other BH3-only proteins, such as Puma, Bmf, Hrk, and Bid, bound more weakly to SPPV14 (Table 1). No binding was detected with Noxa, Bik, or Bad when tested at the highest peptide concentration (2 μM), and these findings were confirmed *in vivo* in immunoprecipitation assays (Fig. 7A) for Bim, Bid, Puma, Bad, and Bmf.

Compared to the binding profiles observed for other prosurvival Bcl-2 proteins (Fig. 6 and Table 1), SPPV14 was found to be unique. Whereas both M11L and SPPV14 engaged Bim, Bak, and Bax, SPPV14 also showed significant affinity for Puma, Hrk, and Bmf (Table 1). In accordance with the *in vitro* binding assay, the BH3-only proteins Bim, tBid, and Puma, which could bind SPPV14, also countered its prosurvival effect when overexpressed in MEFs (Fig. 6E). Unlike SPPV14, M11L cannot bind Puma, and its prosurvival effect was thus not countered by Puma overexpression in MEFs. Moreover, the pattern observed for SPPV14 is distinct from that observed with the two broad classes of mammalian prosurvival Bcl-2 proteins exemplified by Bcl-x_L and Mcl-1 (Fig. 6). The unique pattern observed with SPPV14 may well reflect the specific functional requirements for such an inhibitor in the context of a viral infection.

SPPV14 can functionally antagonize cell death mediated by Bax or Bak. Since SPPV14 can bind both Bax and Bak *in vitro* (Fig. 6) and these findings were confirmed *in vivo* in immunoprecipi-

TABLE 1 Binding affinities of selected prosurvival Bcl-2 proteins for BH3 ligands

BH3 ligand	Binding affinity (IC_{50}[a] in nM)							
	SPPV14	M11L	BHRF1	Bcl-2	Bcl-w	Bcl-x_L	Mcl-1	A1
Bad	>2,000	>1,000	>2,000	16	30	5.3	>100,000	15,000
Bid	341 ± 16	100	42	6,800	40	82	2,100	1
Bik	>2,000	>1,000	>2,000	850	12	43	1,700	58
Bim	26 ± 4	5	<50	2.6	4.3	4.6	2.4	1
Bmf	67 ± 6	100	>2,000	3	9.8	9.7	1,100	180
Hrk	63 ± 6	>1,000	>1,000	320	49	3.7	370	46
Noxa	>2,000	>1,000	>2,000	>100,000	>100,000	>100,000	24	20
Puma	65 ± 1	>1,000	<50	3.3	5.1	6.3	5	1
Bak	46 ± 3	50	NA	>1,000	500	50	10	NA
Bax	32 ± 5	75	NA	100	58	130	12	NA
Bim2A	>1,000	NA	NA	>10,000	>10,000	>10,000	19	520
ABT-737	>1,000	NA	>20,000	3.5	9.5	5.7	>2,000	>2,000

[a] IC_{50}s were determined by solution competition assays using the Biacore optical biosensor (9) and represent means ± SD from 3 independent experiments. NA, not available. Apart from SPPV14, data were taken from references 9, 22, 40* to 42*, and 67*.

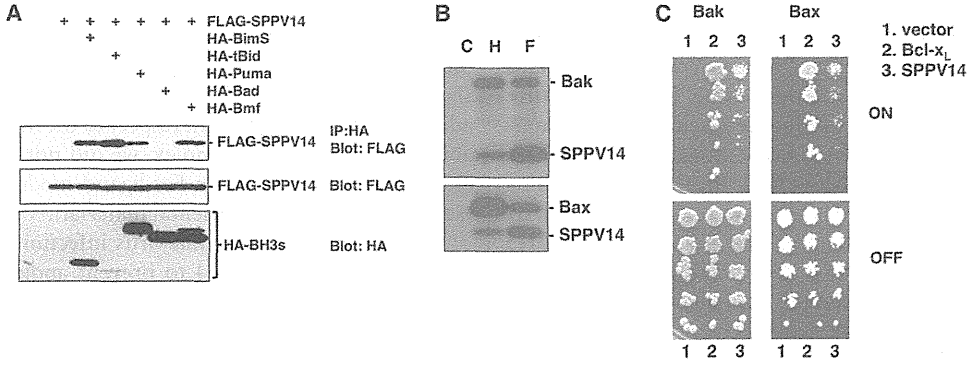

FIG 7 SPPV14 binds both Bak and Bax in mammalian cells and counters growth suppression of yeast by Bax and Bak. (A) Interactions between overexpressed FLAG-SPPV14 and HA-tagged Bim_S, tBid, Puma, Bad, and Bmf were evaluated by coimmunoprecipitation. Equivalent CHAPS-containing 293T cell lysates were immunoprecipitated with antibodies to the HA tag, subjected to SDS-PAGE, and analyzed by Western blotting using anti-FLAG antibody. (B) Interactions between overexpressed FLAG-SPPV14 and HA-tagged Bak or Bax were evaluated by coimmunoprecipitation. Equivalent ^{35}S-labeled CHAPS-containing 293T cell lysates were immunoprecipitated with antibodies to FLAG (F), HA (H), or control (C) tags. (C) SPPV14 counters growth suppression of yeast by Bak and Bax. Yeasts cotransformed with plasmids encoding the indicated prosurvival proteins and Bak or Bax, each under the control of an inducible (GAL) promoter, were spotted onto repressing glucose (OFF) or inducing galactose (ON) plates as 5-fold serial dilutions. The images are representative of 2 independent experiments.

tation assays (Fig. 7B), we next determined if SPPV14 could counter Bax and Bak directly. We utilized a yeast-based assay, where overexpression of Bax or Bak leads to yeast growth arrest (37) that can be overcome by overexpression of mammalian prosurvival Bcl-2 proteins. SPPV14 can counter the growth suppression in yeast cells when either Bax or Bak is overexpressed (Fig. 7C). Thus, we surmise that this most likely reflects direct binding, since yeast cells do not express recognizable Bcl-2 family members. Furthermore, SPPV14 specifically blocks Bax- or Bak-mediated cell death, since expressing SPPV14 in cells deficient in either of the cell death mediators Bak or Bax counters apoptosis (Fig. 8A). Furthermore, when all the endogenous mammalian prosurvival proteins in MEFs were inactivated (Fig. 8B) by a combination of the Bim variant Bim_S2A, which selectively targets Mcl-1 (43), and the BH3 mimetic compound ABT-737 (to target Bcl-2, Bcl-x_L, and Bcl-w and spare SPPV14 [Table 1]) (58), expression of SPPV14 maintained cell viability (Fig. 8C), consistent with the notion that it can directly inhibit Bax or Bak. This capacity to restrain Bax and Bak is presumably dependent on how much SPPV14 is sequestered by those BH3-only proteins that target it (Fig. 6 and Table 1), since overexpression of Bim, tBid, and Puma neutralizes the antiapoptotic effect of SPPV14 (Fig. 6E) in colony-forming assays.

In summary, our studies identified SPPV14 as a novel direct inhibitor of Bax and Bak. It also has a highly distinctive binding profile for the proapoptotic Bcl-2 family proteins expressed in mammals.

DISCUSSION

Apoptosis is a potent defense mechanism deployed by higher organisms against viruses, and in turn, viruses have evolved an astonishing array of strategies to ensure their successful proliferation, propagation, and survival (23, 51). Bcl-2-like proteins from numerous viruses, including structural homologs recently recognized in poxviruses (40, 42), have been shown to be of critical importance for subverting host apoptotic defenses. Consequently, loss of viral Bcl-2 proteins often results in apoptosis upon viral infection, as observed for myxoma virus M11L (59) and vaccinia virus F1L (63).

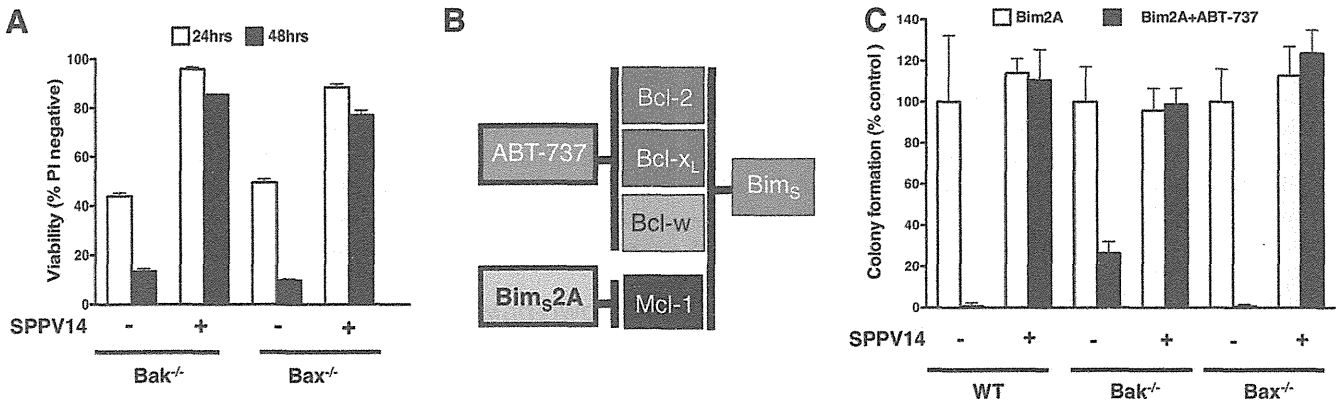

FIG 8 SPPV14 inhibits both Bax and Bak and functionally compensates for endogenous prosurvival Bcl-2. (A) SPPV14 inhibits both Bak- and Bax-mediated apoptosis. Shown is the viability of SPPV14-expressing Bak- or Bax-deficient MEFs treated for 24 h or 48 h with etoposide (10 mM). (B) Selectivity of BH3-only proteins for mammalian prosurvival Bcl-2 proteins (9, 58). (C) SPPV14 potently inhibits apoptosis even if all endogenous mammalian prosurvival Bcl-2 proteins are neutralized. Shown is colony formation of parental or SPPV14-expressing wild-type or Bax- or Bak-deficient MEFs infected with the Mcl-1-selective ligand Bim_S2A (43) and cotreated with ABT-737 (1 μM), a combination that inactivates all endogenous mammalian prosurvival proteins expressed in MEFs (9, 67). The data in panels A and C represent means and SD from 2 independent experiments using a clone of each genotype.

Here, we report the identification and characterization of a novel subgroup of vBcl-2 proteins, the founding members being myxoma virus M11L (25, 40) and vaccinia virus F1L (42, 63). Like the M11L gene, all the novel genes we identified encode putative proteins that bear little primary sequence resemblance to mammalian prosurvival Bcl-2 proteins. Even though the overall sequence similarity to M11L is also low, the critical residues forming the canonical binding grove in M11L (40) were conserved in all six proteins, strongly suggesting the presence of an analogous BH3 binding grove in these proteins (Fig. 1 and 2). Despite the presence of these critical residues, unexpectedly, not all 6 identified M11L orthologs harbored antiapoptotic activity (Fig. 2D). SPV12 (from swinepox virus), gp011L (from shope fibroma virus), and DPV084 (from deerpox virus) did not inhibit etoposide-induced apoptosis when expressed in MEFs. Close inspection of the residues in the putative binding grooves of all six orthologs suggests that four residues, M52, T67, L68, and A71, as a group may determine antiapoptotic activity (see Fig. S1 in the supplemental material). Notably, the only sequence differences between DPV83 and -84 are T25M, A71S, and A101T. With A71 located in the putative binding grove, it is tempting to speculate that the A71S substitution is responsible for the observed difference in antiapoptotic activity. Although the finding that not all six identified M11L orthologs are antiapoptotic was unexpected, it is well established that simple fold conservation in the case of Bcl-2-like proteins is not sufficient for maintaining function. As shown for the vaccinia virus Bcl-2-like proteins A52 and B14 (26), the presence of a Bcl-2 fold does not automatically result in an ability to inhibit Bcl-2-mediated apoptosis. In contrast, both A52 (26) and B14 (10) act on the NF-κB pathway. Similarly, N1L from vaccinia virus also adopts a Bcl-2 fold (2, 12) and acts on NF-κB (7). Importantly, N1L was also shown to inhibit Bcl-2-mediated apoptosis (12), thus displaying dual functionality, which is mediated by two independent sites on the protein (45). It is possible that the three M11L orthologs that were inactive in our apoptosis assays act on NF-κB; however, this remains to be tested experimentally.

In addition to the structure-based sequence analysis, our detailed characterization of sheeppox virus SPPV14 and the previously reported deerpox virus DPV022 (4) support the idea that these viral proteins adopt a Bcl-2-like fold. Like the mammalian prosurvival proteins and myxoma virus M11L, a number of BH3-only proteins can bind SPPV14 (Fig. 6 and Table 1). The binding pattern we observed is unique: Puma can bind and antagonize SPPV14, but not M11L (Fig. 6). Furthermore, SPPV14 can act to directly counter the cell death mediators Bax and Bak, when tested directly (Fig. 7 and 8), in accordance with its ability to bind them (Fig. 6 and Table 1). Considering the similarities in the BH3 domain binding profile and activity against Bax and Bak, the additional ability of SPPV14 to engage Puma, which is absent in M11L, is striking. Among the currently characterized Bcl-2-like proteins from poxviruses, only ORFV125 (65) appears to engage Puma, in addition to Bim, Bik, Hrk, Noxa, and Bax, whereas with F1L (21, 42), N1L (2, 12), and FWPV039 (3, 5), a Puma interaction is not observed. Although the importance of the SPPV14-Puma interaction is currently not established, it is tempting to speculate that, based on the high IC_{50} of 63 nM, the interaction may be functionally relevant.

Functionally, SPPV14 appears to be equipotent to M11L in apoptosis inhibition (Fig. 2 and 3), despite the observed differences in BH3 domain binding. In addition to interactions with Bcl-2 family members (40, 59), M11L has also been reported to form part of the mitochondrial permeability transition pore complex (20) and to intersect with death receptor-mediated apoptosis signaling (59). While it is unclear if SPPV14 also harbors such additional functionality with respect to the mitochondrial permeability transition pore complex, we did not observe an effect of either SPPV14 or M11L on Fas ligand-mediated death signaling (see Fig. S2 in the supplemental material).

In the context of vaccinia virus infection, SPPV14 is able to replace F1L (Fig. 4 and 5) to prevent apoptosis. F1L has been shown to have a highly restricted BH3 binding profile and engages only Bim, Bak, and Bax BH3 domains in biosensor assays (21, 42). Although an interaction with Bax was detected using recombinant protein and peptides, no evidence of a similar interaction in the cellular context has been reported. Functionally, F1L has been shown to engage Bak (48, 61) and Bim (56) and to replace the antiapoptotic activity of Mcl-1 (8), although the precise molecular basis for F1L-mediated apoptosis inhibition remains unclear, with evidence both for (56) and against (18, 50) a role for Bim being reported. Although SPPV14 is able to replace F1L in the context of vaccinia virus, it remains to be established if the mechanism utilized by SPPV14 is similar to the one used by F1L. This is particularly pertinent when considering three issues: first, SPPV14 and F1L ligand binding profiles are substantially different, and second, F1L does not appear to inhibit Bax directly, whereas SPPV14 appears to be M11L-like and to act by neutralizing both Bax and Bak. Third, SPPV14 expression in our experimental system was driven by the strong synthetic poxviral thymidine kinase (17) locus early/late promoter, leading to expression levels and patterns for SPPV14 that are likely to be different from those for endogenous F1L.

Taken together and considering that both vaccinia virus F1L and myxoma virus M11L play key roles for these viruses, we speculate that SPPV14 performs a similar role in sheeppox virus. Key sequence regions in the Bcl-2 family that regulate apoptosis are typically highly conserved. In sheep, Bim harbors two amino acid substitutions at the periphery of the BH3 domain, whereas the Bax BH3 domain is fully conserved, suggesting that at least the SPPV14 interactions with Bim and Bax are likely to be relevant in the context of the sheeppox virus natural host.

By using M11L as bait, we identified a family of novel antiapoptotic factors expressed by poxviruses. Our functional and biophysical characterization of sheeppox virus SPPV14 strongly suggested that SPPV14 adopts a Bcl-2 fold in spite of scant sequence similarity. Interestingly, while SPPV14 seems to play a prominent role in apoptosis inhibition, it does not impact upon the activity of NF-κB, unlike certain other vBcl-2 proteins expressed by vaccinia virus (26). Thus, we anticipate that the detailed characterization of vBcl-2 proteins, such as SPPV14, will continue to unravel the processes that control essential cellular functions in higher organisms.

ACKNOWLEDGMENTS

We thank J. Fletcher, M. Hinds, S. L. Khaw, B. Smith, and M. Yabal for discussions; Abbott Laboratories for ABT-737; F. Battye, J. Blyth, A. Georgiou, H. Ierino, and A. Wardak for excellent technical assistance; and P. Bouillet, D. Fairlie, S. Gerondakis, E. Lee, H. Rabinowich, and A. Strasser for reagents.

Our work is supported by the ARC (fellowship to T.O.), the Cancer Council of Victoria (fellowships to P.M.C.), the Australian National Health and Medical Research Council (program grant 461221; fellow-

ships to P.M.C., D.C.S.H., and M.K.; and IRIISS grant 361646), the Leukemia and Lymphoma Society (SCOR grant 7413; fellowship to M.K.), the Australian Cancer Research Foundation, the Victorian State Government (OIS grant), the Natural Sciences and Engineering Research Council of Canada (graduate scholarship to S.C.), the Alberta Heritage Foundation for Medical Research (studentship to S.C.), the Canadian Institutes of Health Research, the Howard Hughes Medical Institute, and Alberta Innovates Health Solutions. M.B. is a Tier I Canada Research Chair, a Senior Scholar of Alberta Innovates Health Solutions, and a Howard Hughes Medical Institute Scholar in Infection and Parasitology.

REFERENCES

1. **Afonso CL, et al.** 2000. The genome of fowlpox virus. J. Virol. 74:3815–3831.
2. **Aoyagi M, et al.** 2007. Vaccinia virus N1L protein resembles a B cell lymphoma-2 (Bcl-2) family protein. Protein Sci. 16:118–124.
3. **Banadyga L, Gerig J, Stewart T, Barry M.** 2007. Fowlpox virus encodes a Bcl-2 homologue that protects cells from apoptotic death through interaction with the proapoptotic protein Bak. J. Virol. 81:11032–11045.
4. **Banadyga L, et al.** 2010. Deerpox virus encodes an inhibitor of apoptosis that regulates Bak and Bax. J. Virol. 85:1922–1934.
5. **Banadyga L, Veugelers K, Campbell S, Barry M.** 2009. The fowlpox virus BCL-2 homologue, FPV039, interacts with activated Bax and a discrete subset of BH3-only proteins to inhibit apoptosis. J. Virol. 83:7085–7098.
6. **Barry M, et al.** 2000. Granzyme B short-circuits the need for caspase 8 activity during granule-mediated cytotoxic T-lymphocyte killing by directly cleaving Bid. Mol. Cell. Biol. 20:3781–3794.
7. **Bartlett N, Symons JA, Tscharke DC, Smith GL.** 2002. The vaccinia virus N1L protein is an intracellular homodimer that promotes virulence. J. Gen. Virol. 83:1965–1976.
8. **Campbell S, Hazes B, Kvansakul M, Colman P, Barry M.** 2010. Vaccinia virus F1L interacts with Bak using highly divergent Bcl-2 homology domains and replaces the function of Mcl-1. J. Biol. Chem. 285:4695–4708.
9. **Chen L, et al.** 2005. Differential targeting of pro-survival Bcl-2 proteins by their BH3-only ligands allows complementary apoptotic function. Mol. Cell 17:393–403.
10. **Chen RA, Ryzhakov G, Cooray S, Randow F, Smith GL.** 2008. Inhibition of IkappaB kinase by vaccinia virus virulence factor B14. PLoS Pathog. 4:e22. doi:10.1371/journal.ppat.0040022.
11. **Cleary ML, Smith SD, Sklar J.** 1986. Cloning and structural analysis of cDNAs for *bcl*-2 and a hybrid *bcl*-2/immunoglobulin transcript resulting from the t(14;18) translocation. Cell 47:19–28.
12. **Cooray S, et al.** 2007. Functional and structural studies of the vaccinia virus virulence factor N1 reveal a Bcl-2-like anti-apoptotic protein. J. Gen. Virol. 88:1656–1666.
13. **Cuconati A, White E.** 2002. Viral homologs of BCL-2: role of apoptosis in the regulation of virus infection. Genes Dev. 16:2465–2478.
14. **Dewson G, Snowden RT, Almond JB, Dyer MJ, Cohen GM.** 2003. Conformational change and mitochondrial translocation of Bax accompany proteasome inhibitor-induced apoptosis of chronic lymphocytic leukemic cells. Oncogene 22:2643–2654.
15. **DiPerna G, et al.** 2004. Poxvirus protein N1L targets the I-kappaB kinase complex, inhibits signaling to NF-kappaB by the tumor necrosis factor superfamily of receptors, and inhibits NF-kappaB and IRF3 signaling by Toll-like receptors. J. Biol. Chem. 279:36570–36578.
16. **Douglas AE, Corbett KD, Berger JM, McFadden G, Handel TM.** 2007. Structure of M11L: a myxoma virus structural homolog of the apoptosis inhibitor, Bcl-2. Protein Sci. 16:695–703.
17. **Earl PL, Moss B, Wyatt LS, Carroll MW.** 1998. Generation of recombinant vaccinia viruses, p 16.17.11–16.17.19. *In* Ausubel FM, et al (ed), Current protocols in molecular biology. Wiley Interscience, New York, NY.
18. **Eitz Ferrer P, et al.** 2011. Induction of Noxa-mediated apoptosis by modified vaccinia virus Ankara depends on viral recognition by cytosolic helicases, leading to IRF-3/IFN-beta-dependent induction of pro-apoptotic Noxa. PLoS Pathog. 7:e1002083. doi:10.1371/journal.ppat.1002083.
19. **Everett H, et al.** 2000. M11L: a novel mitochondria-localized protein of myxoma virus that blocks apoptosis of infected leukocytes. J. Exp. Med. 191:1487–1498.
20. **Everett H, et al.** 2002. The myxoma poxvirus protein, M11L, prevents apoptosis by direct interaction with the mitochondrial permeability transition pore. J. Exp. Med. 196:1127–1139.
21. **Fischer SF, et al.** 2006. Modified vaccinia virus Ankara protein F1L is a novel BH3-domain binding protein and acts together with the early viral protein E3L to block virus-associated apoptosis. Cell Death Differ. 13:109–118.
22. **Fletcher JI, et al.** 2008. Apoptosis is triggered when prosurvival Bcl-2 proteins cannot restrain Bax. Proc. Natl. Acad. Sci. U. S. A. 105:18081–18087.
23. **Galluzzi L, Brenner C, Morselli E, Touat Z, Kroemer G.** 2008. Viral control of mitochondrial apoptosis. PLoS Pathog. 4:e1000018. doi:10.1371/journal.ppat.1000018.
24. **Goldmacher VS, et al.** 1999. A cytomegalovirus-encoded mitochondria-localized inhibitor of apoptosis structurally unrelated to bcl-2. Proc. Natl. Acad. Sci. U. S. A. 96:12536–12541.
25. **Graham KA, Opgenorth A, Upton C, McFadden G.** 1992. Myxoma virus M11L ORF encodes a protein for which cell surface localization is critical in manifestation of viral virulence. Virology 191:112–124.
26. **Graham SC, et al.** 2008. Vaccinia virus proteins A52 and B14 share a Bcl-2-like fold but have evolved to inhibit NF-kappaB rather than apoptosis. PLoS Pathog. 4:e1000128. doi:10.1371/journal.ppat.1000128.
27. **Green DR, Kroemer G.** 2004. The pathophysiology of mitochondrial cell death. Science 305:626–629.
28. **Griffiths GJ, et al.** 1999. Cell damage-induced conformational changes of the pro-apoptotic protein Bak in vivo precede the onset of apoptosis. J. Cell Biol. 144:903–914.
29. **Hawkins CJ, Wang SL, Hay BA.** 1999. A cloning method to identify caspases and their regulators in yeast: identification of Drosophila IAP1 as an inhibitor of the Drosophila caspase DCP-1. Proc. Natl. Acad. Sci. U. S. A. 96:2885–2890.
30. **Henderson S, et al.** 1993. Epstein virus-coded BHRF I protein, a viral homologue of Bcl-2 protects human B cells from programmed cell death. Proc. Natl. Acad. Sci. U. S. A. 90:8479–8483.
31. **Hsu Y-T, Youle RJ.** 1998. Bax in murine thymus is a soluble monomeric protein that displays differential detergent-induced conformations. J. Biol. Chem. 273:10777–10783.
32. **Huang DC, et al.** 1999. Activation of Fas by FasL induces apoptosis by a mechanism that cannot be blocked by Bcl-2 or Bcl-x_L. Proc. Natl. Acad. Sci. U. S. A. 96:14871–14876.
33. **Huang DCS, Cory S, Strasser A.** 1997. Bcl-2, Bcl-X_L and adenovirus protein E1B19kD are functionally equivalent in their ability to inhibit cell death. Oncogene 14:405–414.
34. **Huang DCS, O'Reilly LA, Strasser A, Cory S.** 1997. The anti-apoptosis function of Bcl-2 can be genetically separated from its inhibitory effect on cell cycle entry. EMBO J. 16:4628–4638.
35. **Huang Q, Petros AM, Virgin HW, Fesik SW, Olejniczak ET.** 2002. Solution structure of a Bcl-2 homolog from Kaposi sarcoma virus. Proc. Natl. Acad. Sci. U. S. A. 99:3428–3433.
36. **Huang Q, Petros AM, Virgin HW, Fesik SW, Olejniczak ET.** 2003. Solution structure of the BHRF1 protein from Epstein-Barr virus, a homolog of human Bcl-2. J. Mol. Biol. 332:1123–1130.
37. **Jabbour AM, et al.** 2006. Human Bcl-2 cannot directly inhibit the Caenorhabditis elegans Apaf-1 homologue CED-4, but can interact with EGL-1. J. Cell Sci. 119:2572–2582.
38. **Jurak I, Schumacher U, Simic H, Voigt S, Brune W.** 2008. Murine cytomegalovirus m38.5 protein inhibits Bax-mediated cell death. J. Virol. 82:4812–4822.
39. **Kinsella TM, Nolan GP.** 1996. Episomal vectors rapidly and stably produce high-titer recombinant retrovirus. Hum. Gene Ther. 7:1405–1413.
40. **Kvansakul M, et al.** 2007. A structural viral mimic of prosurvival Bcl-2: a pivotal role for sequestering proapoptotic Bax and Bak. Mol. Cell 25:933–942.
41. **Kvansakul M, et al.** 2010. Structural basis for apoptosis inhibition by Epstein-Barr virus BHRF1. PLoS Pathog. 6:e1001236. doi:10.1371/journal.ppat.1001236.
42. **Kvansakul M, et al.** 2008. Vaccinia virus anti-apoptotic F1L is a novel Bcl-2-like domain-swapped dimer that binds a highly selective subset of BH3-containing death ligands. Cell Death Differ. 15:1564–1571.
43. **Lee EF, et al.** 2008. A novel BH3 ligand that selectively targets Mcl-1 reveals that apoptosis can proceed without Mcl-1 degradation. J. Cell Biol. 180:341–355.
44. **Liu X, Dai S, Zhu Y, Marrack P, Kappler JW.** 2003. The structure of a Bcl-x_L/Bim fragment complex: implications for Bim function. Immunity 19:341–352.
45. **Maluquer de Motes C, et al.** 2011. Inhibition of apoptosis and NF-